iScience

CellPress
OPEN ACCESS

Article

Methylated histones on mitotic chromosomes promote topoisomerase IIα function for high fidelity chromosome segregation

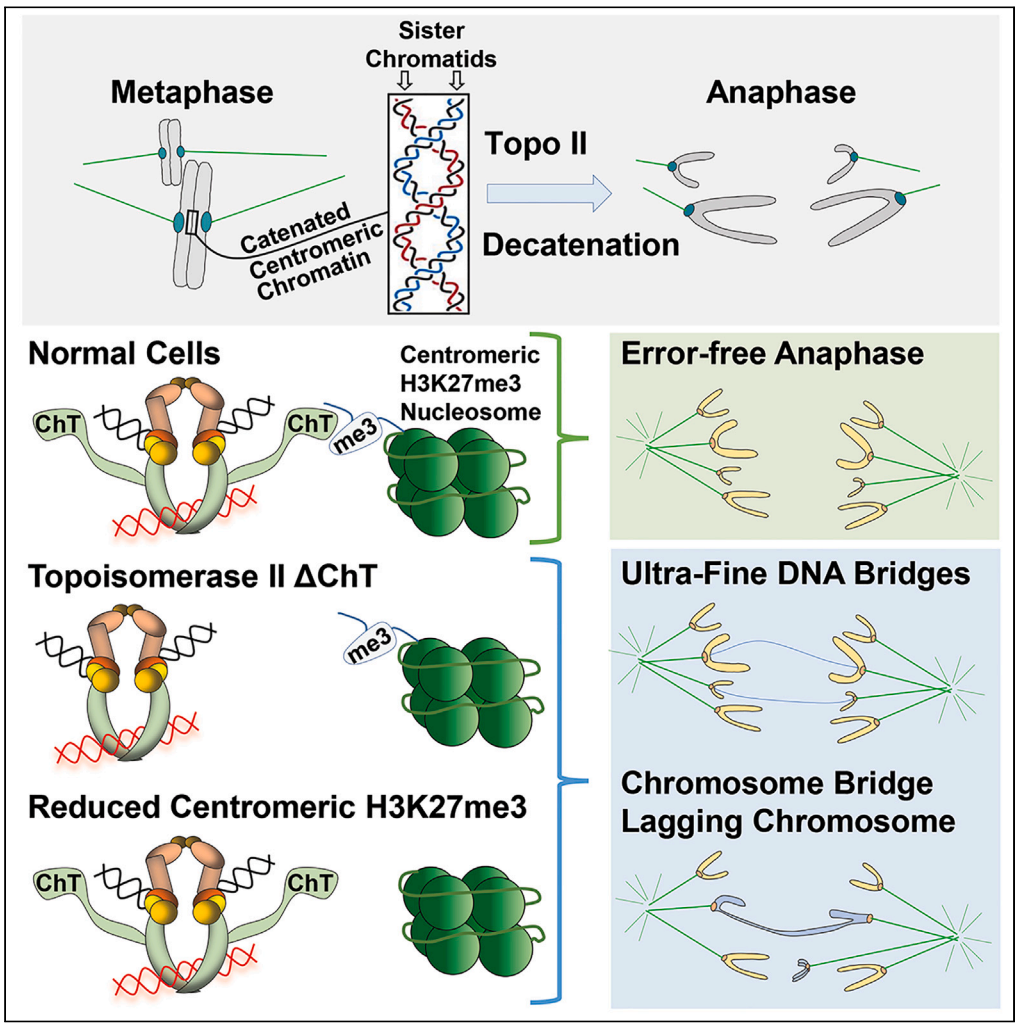

Sanjana Sundararajan, Hyewon Park, Shinji Kawano, ..., Daniel Keifenheim, Duncan J. Clarke, Yoshiaki Azuma

clark140@umn.edu (D.J.C.)
azumay@ku.edu (Y.A.)

Highlights

Chromatin tether domain of topoisomerase IIα ensures complete genome resolution

Topoisomerase IIα interacts with chromatin via methylated nucleosomes

Dynamic histone methylation facilitates sister centromere separation in mitosis

Sundararajan et al., iScience *26*, 106743
May 19, 2023
https://doi.org/10.1016/j.isci.2023.106743

iScience

CellPress
OPEN ACCESS

Article

Methylated histones on mitotic chromosomes promote topoisomerase IIα function for high fidelity chromosome segregation

Sanjana Sundararajan,[1,7] Hyewon Park,[1,7] Shinji Kawano,[2] Marnie Johansson,[3] Bunu Lama,[1] Tomoko Saito-Fujita,[4] Noriko Saitoh,[4] Alexei Arnaoutov,[5] Mary Dasso,[5] Zhengqiang Wang,[6] Daniel Keifenheim,[3] Duncan J. Clarke,[3,*] and Yoshiaki Azuma[1,8,*]

SUMMARY

DNA Topoisomerase IIα (TopoIIα) decatenates sister chromatids, allowing their segregation in mitosis. Without the TopoIIα Strand Passage Reaction (SPR), chromosome bridges and ultra-fine DNA bridges (UFBs) arise in anaphase. The TopoIIα C-terminal domain is dispensable for the SPR *in vitro* but essential for mitotic functions *in vivo*. Here, we present evidence that the Chromatin Tether (ChT) within the CTD interacts with specific methylated nucleosomes and is crucial for high-fidelity chromosome segregation. Mutation of individual αChT residues disrupts αChT-nucleosome interaction, induces loss of segregation fidelity and reduces association of TopoIIα with chromosomes. Specific methyltransferase inhibitors reducing histone H3 or H4 methylation decreased TopoIIα at centromeres and increased segregation errors. Methyltransferase inhibition did not further increase aberrant anaphases in the ChT mutants, indicating a functional connection. The evidence reveals novel cellular regulation whereby TopoIIα specifically interacts with methylated nucleosomes via the αChT to ensure high-fidelity chromosome segregation.

INTRODUCTION

During mitosis, the products of DNA replication are meticulously partitioned between daughter cells. This requires structural re-organization and complete decatenation of the sister chromatids. Topoisomerase IIα (TopoIIα) is an essential enzyme that performs these processes using a unique Strand Passage Reaction (SPR).[1] However, it is not understood how cells coordinate SPR activity to ensure every catenation is resolved for faithful chromosome segregation.

Vertebrates express two isoforms of topoisomerase II (TopoIIα and TopoIIβ), encoded by separate genes. Owing to conserved ATPase domains and catalytic cores, they show similar SPR activity *in vitro*.[2] However, their C-terminal Domains (CTDs), with much lower homology, distinguish the isoforms and account for diversity in their cellular functions: TopoIIα is essential for mitotic chromosome organization and segregation, whereas TopoIIβ is dispensable for mitosis but has crucial roles in transcription, particularly in non-dividing cells.[3–5]

The TopoIIα CTD has distinct regions interacting with DNA and histones. Binding of αCTD to linker DNA was implicated in controlling chromatin loop length which is essential for shaping condensed chromosomes in Xenopus egg extracts.[6,7] Loss of the αCTD also reduced TopoIIα activity in egg extracts, suggesting the αCTD contributes to decatenation under physiological conditions. In contrast, the last 31 αCTD residues (named the Chromatin Tether domain; ChT) are required for direct interaction with recombinant histone H3 and with methylated H3 N-terminal tails.[8] αCTD lacking the ChT retains interaction with DNA suggesting a modest role of the ChT in DNA binding.[8] TopoIIα concentrates as centromeres in mitosis, and analysis of centromere-specific histone modifications revealed prominent methylation of H3 and H4 N-terminal tails.[9] Although it is not known if methylated centromeric histones function in mitosis, the data raise the possibility that interaction of αChT with specific nucleosomes contributes to chromosome segregation.

[1]Department of Molecular Biosciences, University of Kansas, Lawrence, KS 66045, USA

[2]Department of Biochemistry, Faculty of Science, Okayama University of Science, Okayama 700-0081, Japan

[3]Department of Genetics, Cell Biology and Development, University of Minnesota, Minneapolis, MN 55455, USA

[4]Division of Cancer Biology, The Cancer Institute of Japanese Foundation for Cancer Research, Tokyo 135-8550, Japan

[5]Division of Molecular and Cellular Biology, National Institute for Child Health and Human Development, National Institutes of Health, Bethesda, MD 20892-4480, USA

[6]Center for Drug Design, College of Pharmacy, University of Minnesota, Minneapolis, MN 55455, USA

[7]These authors contributed equally

[8]Lead contact

*Correspondence: clark140@umn.edu (D.J.C.), azumay@ku.edu (Y.A.)

https://doi.org/10.1016/j.isci.2023.106743

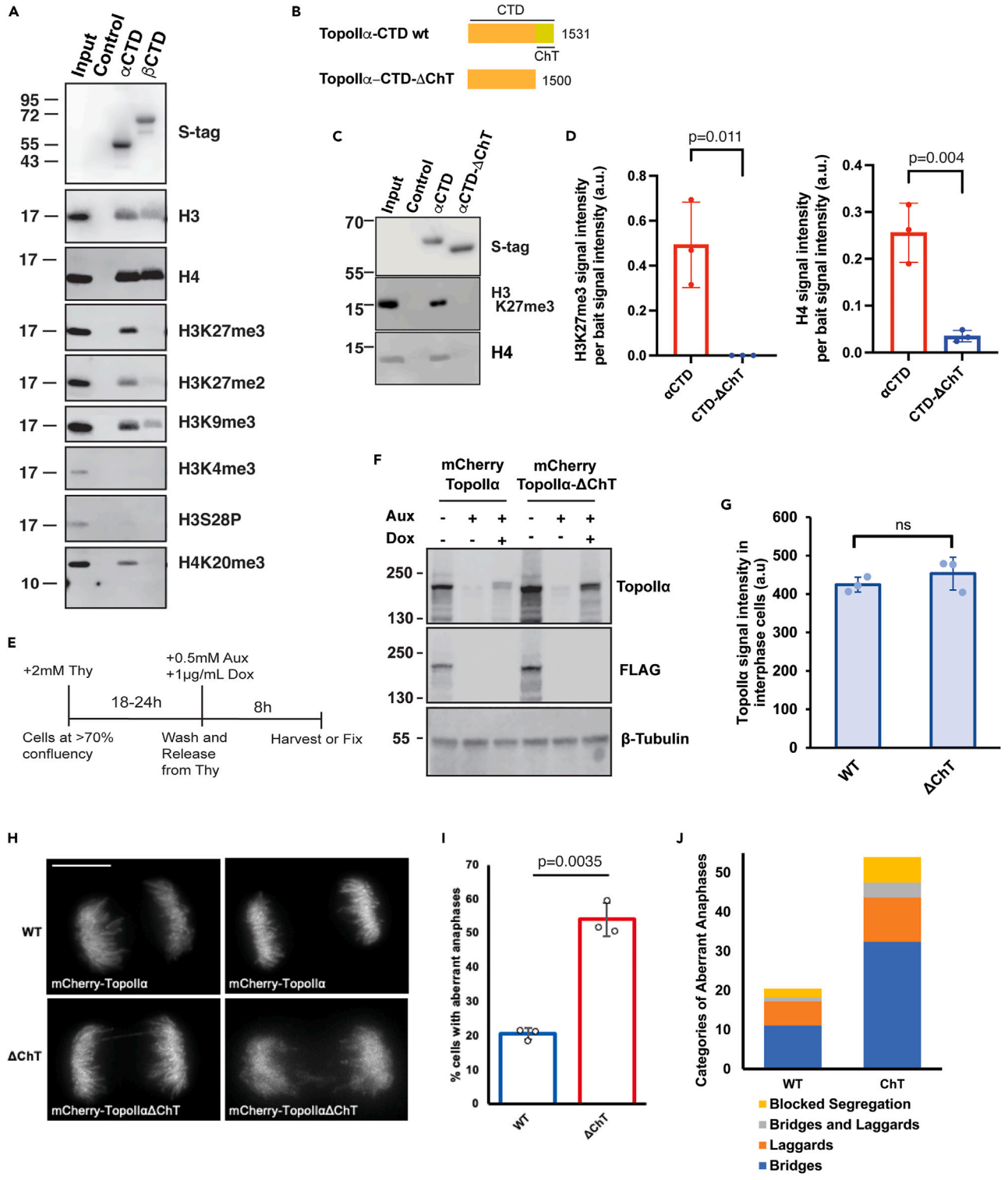

Figure 1. The TopoIIα ChT domain is required for interaction with methylated mono-nucleosomes and for accurate chromosome segregation

(A) Western blots showing precipitation of mono-nucleosomes from human cell extracts by recombinant TopoIIα-CTD (αCTD) or TopoIIβ-CTD (βCTD) proteins.

(B) Representation of the primary structure of the TopoIIα C-terminal domain (CTD) and a mutant version lacking the ChT (highlighted in yellow).

Figure 1. *Continued*

(C) Western blots showing precipitation of mono-nucleosomes from human cell extracts by recombinant TopoIIα-CTD (αCTD) or TopoIIα-CTD-ΔChT (αCTD-ΔChT) proteins.

(D) Quantification of H3K27me3 signal intensity (left) and H4 signal intensity (right) per bait signal intensity (a.u.) from panel C. n = 3 experiments. p-values indicate two-tailed unpaired samples t-tests. Error bars indicate SD.

(E) Scheme for cell synchronization to analyze effects of TopoIIα using the AID system (for data in panels F-J).

(F) Western blot of whole cell extracts showing depletion of endogenous TopoIIα (tagged with FLAG) on Aux addition, and replacement with mCherry-TopoIIα or mCherry-TopoIIα-ΔChT upon Dox addition in engineered DLD-1 cells, following the scheme in panel E.

(G) Quantification of mCherry-TopoIIα signal intensity in interphase nuclei in live cells (from >295 cells for each cell line analyzed over three independent experiments). Error bars indicate SD. Filled circles show means from each experimental repeat. p-value indicates two-tailed unpaired samples t-test. ns: not statistically significant.

(H) Images of anaphase cells analyzed at the first mitosis after treatment as in panel E. Bars, 5μm.

(I) Quantification of cells with aberrant anaphases (chromosome bridges and laggards) in mCherry-TopoIIα or mCherry-TopoIIα-ΔChT at the first mitosis after treatment as in panel E. Experiment was performed three times; WT, n = 140 cells; ΔChT, n = 266 cells. Filled circles show means from each experimental repeat. p-value indicates two-tailed unpaired samples t-test. Error bars indicate SD.

(J) Aberrant mitoses observed in H and I were categorized into four groups. Plot shows the percentage for each category. The numbers of bridged and/or lagging chromosomes in each anaphase cell examined are plotted in Figure S3.

Here, we used the auxin inducible degron (AID) system coupled with doxycycline inducible (Tet-ON) gene replacement in DLD-1 cells to reveal a critical function of the TopoIIα ChT in mitotic chromosome segregation. We show that αChT interacts with mono-nucleosomes containing H3K27me3 and/or H4K20me3. Inhibiting methyltransferases that target these residues reduced centromeric TopoIIα and increased chromosome segregation errors. The composition of aromatic amino acids within the αChT was critical for interaction with methylated nucleosomes and for limiting segregation errors. The data reveal a novel role of H3K27 and H4K20 methylation in promoting the mitotic function of TopoIIα to ensure faithful chromosome segregation.

RESULTS

TopoIIα interacts with methylated nucleosomes through the ChT domain

The ability of αCTD to interact with DNA and bind directly to recombinant Histone H3 suggest nucleosome binding could explain the mitosis specific functions of TopoIIα versus TopoIIβ. We prepared a population of mono-nucleosomes from human nuclear fractions, which were pre-extracted with detergent and 400 mM salt (Figure S1A) and performed pull-down assays using TopoIIα-CTD (αCTD) and TopoIIβ-CTD (βCTD) as bait. Western blotting for Histone H3 and H4 revealed both αCTD and βCTD efficiently precipitate mono-nucleosomes (Figure 1A). Next, we asked if the precipitated mono-nucleosomes possess specific modifications, based on the methylated H3 peptides we observed to interact with αCTD.[8] Because TopoIIα is known to enrich at centromere on mitotic chromosomes, we also examined known modifications that exist at centromeric regions. The N-terminal tails of histone H3/H4 specifically lack acetylation at centromeres and are instead methylated, predominantly at H3K9, H3K27 and H4K20.[9] Of interest, H3K9me3 was observed in both precipitants with αCTD and βCTD, but H3K27me2/me3 and H4K20me3 were observed only with αCTD (Figure 1A). H3K4me3 and H3S28-Phos were absent from both. Because the nucleosome preparations were homogeneous mono-nucleosomes (Figure S1B), interaction with these specifically modified nucleosomes must be direct, rather than bridged by adjacent nucleosomes. Therefore, although αCTD and βCTD interact with native mono-nucleosomes, there are distinct species of nucleosome that bind preferentially. The contribution of αChT was determined using an αChT truncation (αCTD-ΔChT) mutant (Figures 1B–1D). Loss of H4 in precipitates revealed αChT is required for interaction with nucleosomes. This supports previous findings that αChT is required for binding to recombinant H3[8] and suggests that αChT governs the ability of αCTD to interact with nucleosomes in general, regardless of their modification status. Swapping the ChT regions of αCTD and βCTD supported the contribution of αChT in interaction with methylated histone containing chromatin (Figures S1C and S1D). The αCTD with βChT lost enrichment of H3K27me3-containing chromatin in pull-down assays and, in contrast, βCTD with αChT gained enrichment of H3K27me3-containing chromatin (Figures S1C and S1D).

αChT has critical functions in mitosis

αChT preferentially contributes to interaction with specific methylated nucleosomes that are present at centromeres, but whether αChT has a role in chromosome segregation is not firmly established. Previous studies depleted endogenous TopoII using siRNA against both isoforms while inducing a TopoIIα-ΔChT mutant. This revealed sister chromatid resolution and condensation defects.[8] One complication of this

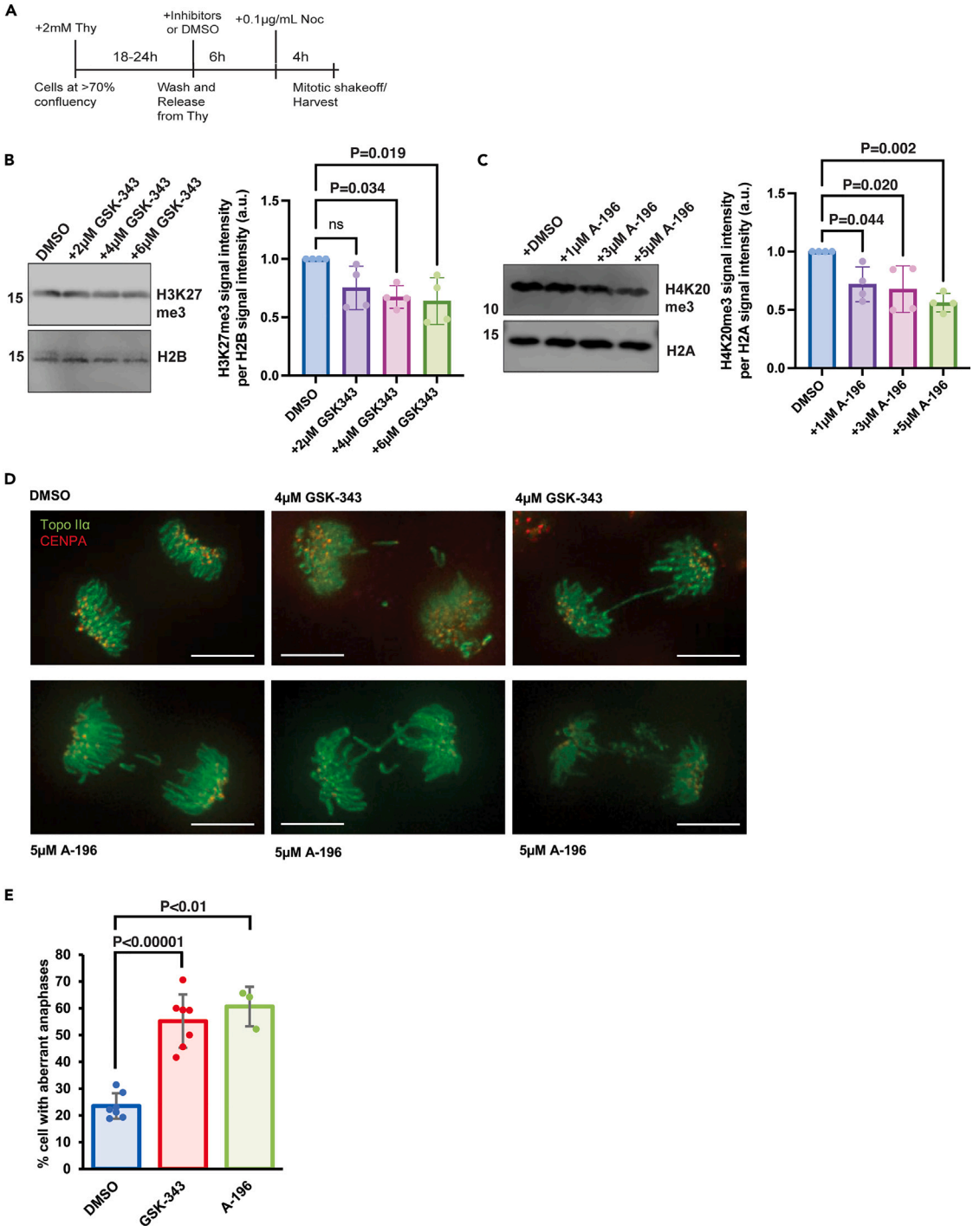

Figure 2. Histone methyl-transferase inhibitors induce chromosome bridges and laggards in anaphase

(A) Scheme for cell synchronization to quantify mitotic H3K27me3 and H4K20me3 levels after treatment with histone methyl-transferase inhibitors within a single cell cycle, from S-phase to mitosis.

(B and C) Western blots of purified mitotic chromosomes after treatment shown in panel A, for H3K27me3 (B) and H4K20me3 (C). Representative gel images are shown in the left panels and quantification of signal intensities are shown in the right panels. p-values indicate one-way ANOVA analysis followed by Tukey multicomparison correction. Horizontal bars indicate means and error bars indicate SD calculated for the means across the four independent experiments. ns: not statistically significant.

Figure 2. *Continued*

(D) Projected images of live mitotic cells showing chromosome bridges and/or lagging chromosomes using a cell line where both endogenous TopoIIα alleles are fused to mNeon at the N-termini (mNeon-TopoIIα) and both endogenous CENP-A alleles are fused miRFP670 (miRFP-CENP-A) (Figure S5). Bars, 5 μm. Cells were treated as in panel A except Nocodazole was omitted and cells were imaged at the first mitosis after treatment.

(E) Quantification of cells with aberrant anaphases (chromosomes bridges or lagging chromosomes) after treatment as in panel D. Numbers of cells counted: DMSO, n = 254; GSK-343, n = 242, A-196, n = 179. p-values indicate two-tailed unpaired samples t-tests. Error bars indicate SD and filled circles show means from each experimental repeat.

approach is the long time frame needed to deplete TopoII (>1 cell cycle) which could lead to secondary effects. To determine the role of αChT at the first mitosis after replacing endogenous TopoIIα with a ΔChT mutant, we utilized AID-mediated TopoIIα-depletion with concomitant expression of various TopoIIα mutants[10] (Figure S2). For these experiments, cells synchronized at the G1/S border were treated with Auxin (Aux) and doxycyline (Dox) on cell cycle resumption (Figure 1E). Endogenous TopoIIα depletion and expression of exogenous mCherry-TopoIIα were confirmed by western blotting (Figure 1F) and consistent expression levels of the transgenes were observed by quantification of mCherry signals from live imaging (Figure 1G), validating this new TopoIIα-replacement system and allowing evaluation of αChT-dependent mitotic functions within a single cell cycle from S-phase to mitosis. Depletion of endogenous TopoIIα without replacement resulted in complete blockage of chromosome segregation (Figures S3A and S3B), consistent with previous studies demonstrating the essential function of TopoIIα in mitosis.[3,8,11,12] Replacing endogenous TopoIIα with the αChT deletion mutant, within a single cell cycle, increased aberrant anaphases including both chromosome bridges and laggards (Figures 1H–1J and S3C), compared with the wild-type replacement. This is consistent with previous observations[8] using siRNA-mediated replacement. The results definitively establish that αChT has critical mitotic functions for accurate chromosome segregation.

Reduced H3K27me3 or H4K20me3 from S-phase to mitosis is accompanied by chromosome mis-segregation

αChT is required for interaction with mono-nucleosomes containing H3K27me3 and/or H4K20me3 and prevents segregation errors. However, because there was almost complete loss of nucleosome interaction in the αChTΔ mutant, any specific contribution of αChT binding to nucleosomes with methylated histones could not be inferred. Moreover, although methylated nucleosomes are enriched at centromeres, their possible roles in mitosis have been scarcely studied. To determine whether H3K27me3 and/or H4K20me3 have roles in chromosome segregation, we treated cells with potent inhibitors of methyltransferases, GSK-343 for H3K27[13] and A-196 for H4K20,[14] from S-phase to mitosis (Figure 2A). Previous studies have shown that abolishing these methylations requires several days treatment with inhibitors. Nevertheless, because inheritance of histone modifications occurs after DNA replication, we reasoned that treatment during this window ought to reduce their abundance and allow analysis of the first mitosis. Indeed, western blotting of mitotic chromosomal fractions showed a dose-dependent reduction of each histone methylation (Figures 2B and 2C). Moreover, both GSK-343 and A-196 increased the incidence of aberrant anaphases (Figures 2D and 2E). GSK-343 did not affect H3K9me3 levels on mitotic chromosomes (Figure S4), supporting specificity of the inhibitor. The data raise the question whether H3K27me3 and H4K20me3 have a functional relationship with αChT-dependent interaction with nucleosomes containing these methylations.

Aromatic αChT residues contribute to methylated nucleosome binding

If the direct interaction observed between recombinant αCTD and synthetic methylated histone tails[8] is governed by the αChT, there could be a hydrophobic pocket composed of aromatic residues within the αChT that allows tri-methylated lysine interaction, as shown for well-established methylated histone binding proteins including HP1 for H3K9me3 and PRC2 for H3K27me3.[15–17] We examined whether αChT aromatic residue substitutions affected interaction with methylated mono-nucleosomes (Figure 3A). All three mutants had reduced interaction with mono-nucleosomes, indicated by reduced H4 and H3 precipitation (Figures 3B and 3C). Among them, Y1521A showed the least binding, a deficit similar to αCTD-ΔChT (Figure 1C). However, F1502A retained nucleosome interaction, albeit much weaker than wt. F1531A had slightly reduced nucleosome interaction compared to wt, but it was not statistically significant. Interaction with H3K27me3-containing nucleosomes was almost abolished in both F1502A and Y1521A. F1531A precipitated significantly less H3K27me3-containing nucleosomes than wt but significantly more than either F1502A or Y1521A. Without structural information about the binding surfaces between histones

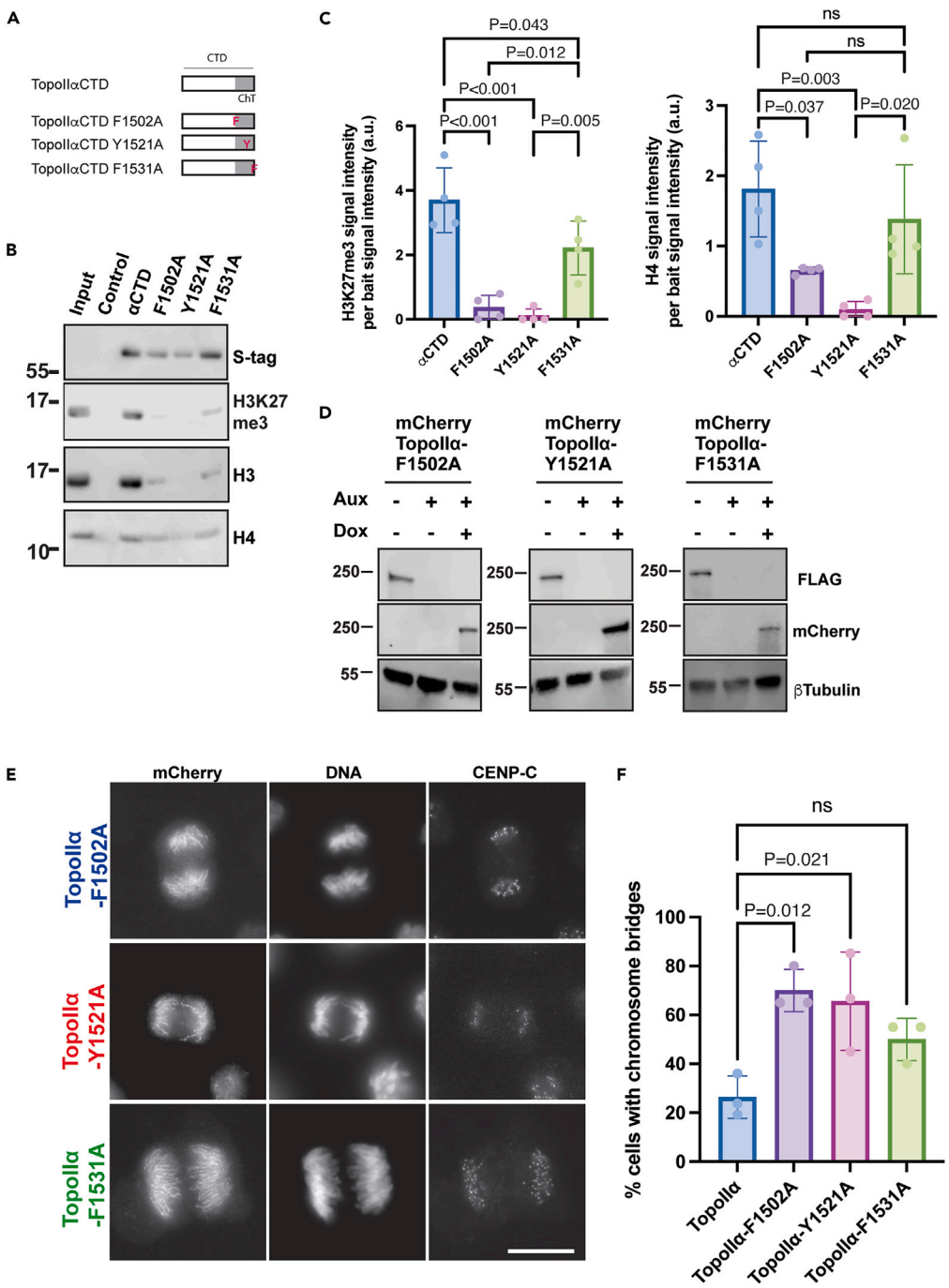

Figure 3. The ability of ChT point mutants to precipitate mono-nucleosomes correlates with their ability to suppress chromosome segregation errors *in vivo*

(A) Representation of the TopoIIα ChT indicating positions of single amino acid substitutions: Phe1502, Tyr1521 and Phe1531 were replaced with Ala (represented as F1502A, Y1521A and F1531A respectively).

(B and C) Western blots (B) showing precipitation of mono-nucleosomes from human cell extracts by each recombinant TopoIIα ChT mutant protein shown in panel A. Graphs (C) quantify the signal intensities per bait signal intensity (a.u.) for Histone H4 and mono-nucleosomes containing H3K27me3. *n* = 4 experiments. p-values indicate one-way ANOVA analysis followed by Tukey multicomparison correction. ns: not statistically significant. Error bars indicate SD.

(D) Western blot of whole cell extracts showing depletion of endogenous TopoIIα (tagged with FLAG) upon Aux addition, and replacement with mCherry-TopoIIα or mCherry-TopoIIα-ChT point mutants upon Dox addition in engineered DLD-1 cells, following the cell synchronization scheme shown in Figure 1E.

Figure 3. *Continued*

(E) Images of anaphase cells analyzed at the first mitosis after treatment as in Figure 1E.

(F) Quantification of cells with aberrant anaphases (chromosome bridges and laggards) in mCherry-TopoIIα or mCherry-TopoIIα ChT point mutants at the first mitosis after treatment as in panel 1E. n = 3 experiments with at least 25 cells counted for each condition. p-values indicate one-way ANOVA analysis. Error bars indicate SD. ns: not statistically significant.

and αChT, these data do not reveal direct contacts with the methylated residues. These results, however, reveal that the mutants are useful tools to investigate αCTD/methylated chromatin interaction and ChT-dependent mitotic functions because they have differential abilities to bind methylated mono-nucleosomes. Therefore, we generated cell lines to replace endogenous TopoIIα with the same mutants (Figures S2 and 3D). Analysis of the first mitosis after S-phase synchrony (Figure 1E) revealed F1502A and Y1521A had significantly increased anaphase errors (Figures 3E and 3F) comparable with TopoIIα-ΔChT and inhibitor treated cells (Figures 1H–1J and 2E). In contrast, F1531A had an increase in errors that was not statistically significant from wt. Therefore, not only do the point mutants increase anaphase errors, but penetrance of their phenotypes correlates with their ability to interact with methylated nucleosomes.

αChT-dependent nucleosome interaction correlates with TopoIIα association with mitotic chromosomes

Previous studies indicated the αChTΔ mutant has reduced affinity for mitotic chromosomes.[8] Therefore, we asked if the aromatic αChT residues required for interaction with methylated nucleosomes are also required for proper chromosomal association. We quantified the mCherry fused to the mutant proteins in live nocodazole arrested cells (Figures 4A and 4B) and in anaphase cells (Figure S6). F1502A and Y1521A had decreased TopoIIα association with chromosomes whereas F1531A, which partially retains methylated nucleosome interaction and had only a marginal increase in aberrant anaphases, did not show a reduction in chromosome association in both pro/metaphase (Figures 4A and 4B) and anaphase (Figure S6). To rule out the possibility that the differences in mitotic chromosomal intensities were due to variations in expression levels, we determined that the interphase nuclei signal intensities (that contain the entire pool of TopoIIα proteins) were similar (Figure 4C). In addition to the quantitative differences in mitotic cells, there were qualitative differences in the localization patterns, where chromosome arm localization appeared more diffuse and centromere enrichment was less obvious than for wt mCherry-TopoIIα (Figure 4A). To gain an unbiased evaluation of these morphologies, we applied the images to a machine leaning algorithm, wndchrm.[18] Initial image-titration analysis showed the classification accuracy was high at 88% with 10 training images of wt and the Y1521A mutant (Figure S7A). We hence collected 30 images from each cell line to randomly subdivide into two sub-groups: WT_1 and WT_2, etc. The resultant eight sub-groups were subjected to wndchrm to measure differences by computing the morphological distances (Figure 4D). As expected, distances between each sub-group of the same protein were small, confirming accuracy of the analysis. The distances of F1502A and Y1521A from wt were large, whereas that of F1531A was far less. The morphological similarity and dissimilarity visualized as a phylogenetic tree (Figure 4E) showed that F1502A and Y1521A were morphologically distant from wt and from each other. First, these trends are consistent with quantification of TopoIIα on mitotic chromosomes, the ability of each mutant to bind nucleosomes and the effects on chromosome segregation. Second, the different morphologies of F1502A and Y1521A may indicate they possess different abilities to bind specific nucleosomes that affect their association with mitotic chromosomes. To determine whether H3K27me3 and H4K20me3 contribute to TopoIIα association with mitotic chromosomes and centromeres, we used a mNEON-TopoIIα miRFP670-CENP-A cell line (Figures S5A–S5C) and the GSK-343 or A-196 treatment conditions in Figure 2. Because the tagged alleles are homozygous, this allowed us to image the entire pool of these endogenous proteins (Figures 4F–4H). CENP-A signals showed no significant changes, but quantification of centromeric TopoIIα revealed a significant reduction after either GSK-343 or A-196 (Figures 4G and 4H). In contrast, wndchrm analysis revealed only subtle differences in global chromosomal localization of TopoIIα (Figures S7 and S8). These results suggest that decreased abundance of H3K27me3 and H4K20me3 modifications that are established from S-phase to mitosis specifically accompanies a reduction in centromeric TopoIIα.

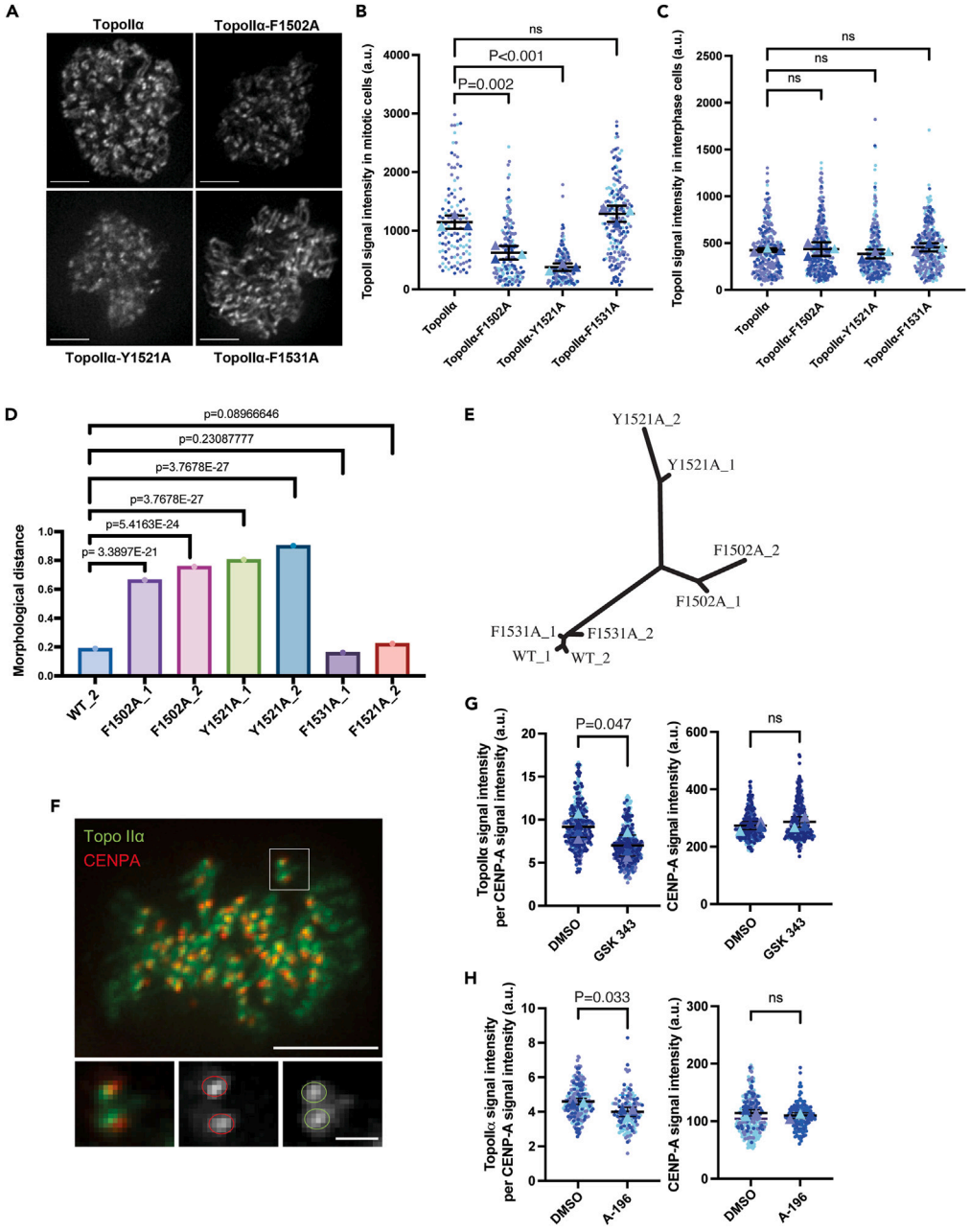

Figure 4. Topoll α ChT mutants localize aberrantly to mitotic chromosomes and inhibitors of histone methyltransferases decrease the abundance of Topoll α at centromeres in live cells

(A) Projected images of mCherry-Topoll α in live mitotic cells. Bars, 5 μm.

(B) Superplots showing quantification of mCherry-Topoll α signal intensity on mitotic chromosomes in live cells (from >100 cells analyzed over three independent experiments). p-values indicate one-way ANOVA analysis followed by Tukey multicomparison correction. Horizontal bars (black) indicate means and error bars indicate SD calculated for the means across the three independent experiments. ns: not statistically significant.

(C) Superplots showing quantification of mCherry-Topoll α signal intensity in interphase nucleus in live cells (from >150 cells analyzed over three independent experiments). p-values indicate one-way ANOVA analysis followed by Tukey multicomparison correction. Horizontal bars (black) indicate means and error bars indicate SD calculated for the means across the three independent experiments. ns: not statistically significant.

(D) Morphological distances computed by wndchrm analysis of Topoll α ChT mutant images compared with wt images (WT_1). Each group was randomly divided into two sub-groups (e.g., for wt; WT_1 and WT_2) to monitor reproducibility

Figure 4. *Continued*

and reliability of the analysis. A larger distance indicates a greater morphological dissimilarity in an image feature space. Although F1502A and Y1521A were distinct from wt TopoIIα, F1531A images were similar to wt.

(E) Phylogenetic tree representing the morphological relationships among the TopoIIα ChT mutants compared to wt. The tree is based on the values obtained from the wndchrm analysis in panel D.

(F) Representative images of live cells with CEN TopoIIα and CENP-A (CEN marker) used for quantification of CEN TopoIIα signal. Bars, 5 μm (larger merged image), 1 μm (magnified images).

(G) Superplots showing quantification of TopoIIα signal intensities at CENs per the corresponding CENP-A signal intensities (*left*) for both DMSO and GSK-343 treatments. DMSO, n = 366 centromeres; GSK-343, n = 413 centromeres (from 3 independent experiments as represented in the plot). p-value indicates two-tailed unpaired samples t-test. Error bars indicate SD. Quantification of CENP-A signal intensities (*right*) used for the analysis in the *left* panel. p value indicates two-tailed unpaired samples t-test. Error bars indicate SD. ns: not statistically significant.

(H) Superplots showing quantification of TopoIIα signal intensities at CENs per the corresponding CENP-A signal intensities (*left*) for both DMSO and A-196 treatments. DMSO, n = 202 centromeres; A-196, n = 129 centromeres (from 3 independent experiments as represented in the plot). p value indicates two-tailed unpaired samples t-test. Error bars indicate SD. Quantification of CENP-A signal intensities (*right*) used for the analysis in *right* panel. p value indicates two-tailed unpaired samples t-test. Error bars indicate SD. ns: not statistically significant.

αChT mutation and decreased H3K27me3/H4K20me3 modification correlate with increased anaphase UFBs

TopoIIα prevents UFBs in anaphase by resolving catenated centromeric DNA.[19,20] Thus, we examined whether αChT and proper H3K27me3/H4K20me3 modifications contribute to this centromere TopoIIα function. We compared the TopoIIα replaced cell lines either before endogenous TopoIIα depletion (-Aux) or after depletion and induction of wt or ChTΔ (+Aux +Dox). The cells were synchronized (Figure 1E) then UFBs quantified at the first mitosis following release (Figures 5A–5C). Before endogenous TopoIIα depletion most cells had no UFBs and there was no difference after depletion and expression of mCherry-TopoIIα wt (Figures 5B and 5C). Therefore, mCherry-TopoIIα rescues the lack of endogenous TopoIIα. In contrast, almost all TopoIIα-ΔChT cells had UFBs and there was an increased number of UFBs/cell (Figures 5B and C). Similarly, treatment of cells from S-phase to mitosis with either GSK-343 or A-196 led to a dose-dependent increase in UFBs/cell (Figure 5D). However, when cells were treated with both inhibitors, an additive effect was not observed either in terms of UFBs/cell or percent UFB-positive cells (Figure 5E). The data suggest αChT and proper H3K27me3/H4K20me3 modification prevent UFBs, and also that H3K27me3/H4K20me3 may contribute to prevent UFBs collaboratively. To estimate the proportion of UFBs that connect centromeres, we scored UFBs that terminate at CENP-A foci (Figure S9). In the TopoIIα replaced cells and inhibitor treated cells, most UFBs terminated at CENP-A foci, indicating that most UFBs originate from catenations at centromeres, though it is technically not possible to rule out catenation of peri-centromeric DNA using this approach. Nevertheless, the data are consistent with the effects the inhibitors had on the abundance of centromeric TopoIIα.

Dynamic H3K27-methylation in mitosis may prevent UFBs

Although the majority of UFBs arise due to persistent catenations, they can result from un-replicated loci.[21] Inhibiting histone methylation during S-phase could have led to the latter type of UFBs. To assess this, mitotic cells were isolated after colcemid treatment, then GSK-343 added for 90 min before release (Figure 5F) and UFBs quantified in live cells (Figures 5G–5I). Strikingly, GSK-343 almost doubled the percentage of cells with UFBs and increased UFBs/cell 2.5-fold (Figures 5H and 5I). Importantly, simultaneous inhibition of the H3K27 demethylase enzymes (UTX/JMJD3) with GSK-J4[22] counteracted the effect of GSK-343 strongly indicating that the effects of GSK-343 were because of altered H3K27me3 levels. Of interest, treatment with GSK-J4 alone increased UFBs similar to GSK-343. Together, the observed increases in UFBs suggested that H3K27me3 dynamics at centromeres of mitotic chromosomes are crucial for accurate chromosome segregation. It is currently not known if H3K27me3 turns over in mitosis. To test this directly, we repeated the above experiment, briefly treating mitotic cells with GSK-343, then immunostained the chromosomes with antibodies to detect centromeres (human CREST serum) and H3K27me3 (Figure 5J). Strikingly, the abundance of H3K27me3 was reduced at centromeres within 90 min treatment with the PRC2 inhibitor (Figures 5K and 5L). The data suggest that ongoing dynamic H3K27 methylation at centromeres plays an important role in TopoIIα-mediated resolution of centromere catenations.

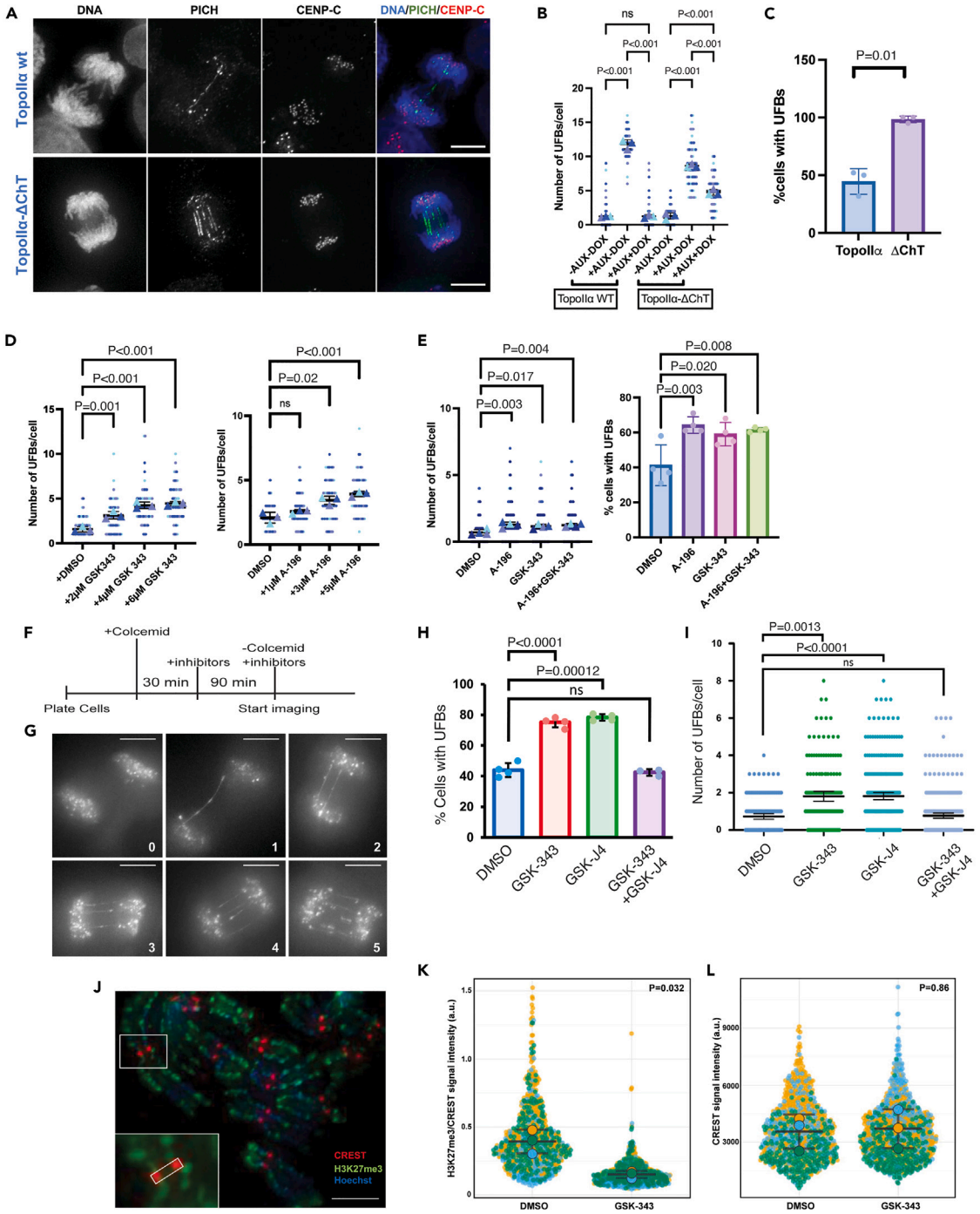

Figure 5. Deletion of the ChT or treatment with histone methyl-transferase inhibitors induces Ultra-Fine DNA Bridges (UFBs) in anaphase

(A–C) Representative images (A) acquired for UFB quantification after replacement of endogenous TopoIIα with either mCherry-TopoIIα (*top*) or mCherry-TopoIIα-ΔChT (*bottom*). Cells were synchronized and treated according to the scheme shown in Figure 1E, then stained with anti-PICH antibody to reveal UFBs and CENP-C antibody to mark centromeres. Bars, 5 μm.

(B) Superplots showing quantification of the number of UFBs/cell (from >60 cells counted over three independent experiments) for TopoIIα-WT replaced cells (left) and TopoIIα-ΔChT replaced cells (right). p-value indicates one-way ANOVA analysis followed by Tukey multicomparison correction for the means. Horizontal bars indicate mean and error bars indicate SD calculated for the means across the three independent experiments. ns: not statistically significant.

(C) Quantification of percent cells with UFBs in the absence of Aux and Dox (i.e., with only endogenous TopoIIα expression) or after treatment with Aux and Dox (i.e., with only mCherry-TopoIIα or mCherry-TopoIIα-ΔChT expression). More than 60 cells were counted over three independent experiments. p value indicates two-tailed unpaired samples t-test. Error bars indicate SD.

Figure 5. *Continued*

(D) Superplots showing quantification of UFBs/cell (from >60 cells counted over three independent experiments) after treatment with dose ranges of either GSK-343 or A-196 histone methyl-transferase inhibitors. Cells were synchronized and treated according to the scheme in Figure 2A (omitting the nocodazole step) then mitotic cells were fixed and stained with anti-PICH antibody to reveal UFBs and CENP-C antibody to mark centromeres. p-values indicate one-way ANOVA analysis followed by Tukey multicomparison correction for the means. ns: not statistically significant.

(E) Quantification of UBFs/cell with single and combined treatments with GSK-343 (4 μM) and A-196 (5 μM). Cells were synchronized and treated as in Figure 2A (omitting the nocodazole step). *Left*, superplots show quantification of UFBs/cell (from >60 cells counted over three independent experiments). Horizontal bars indicate mean values. ns: not statistically significant. *Right*, histogram plots showing percentage of cells with UFBs, using the same data. Filled circles show individual experiment means. Error bars indicate SD calculated for the means across the three independent experiments. p-values in both graphs indicate one-way ANOVA analysis followed by Tukey multicomparison correction for the means.

(F–I) Analysis of UFBs after treatment of mitotic cells with histone methyltransferase (GSK-343) and demethylase (GSK-J4) inhibitors using engineered DLD-1 cells in which both endogenous alleles of PICH were tagged with mNEON (Figure S5).

(F) Scheme showing mitotic synchrony and treatments with GSK-343 (15 μM), GSK-J4 (5 μM) or both in combination. (G) Representative images of anaphases from which UFBs/per cell were quantified. Numbers indicate UFBs/cell. Bars, 5μm.

(H) Quantification of percentage of cells with UFBs. Filled circles show individual experimental means. Error bars indicate SD calculated for the means across the independent experiments. DMSO: n = 153 cells. GSK-343: n = 170 cells. GSK-J4: n = 300 cells. GSK-343 plus GSK-J4: n = 291. p-values indicate one-way ANOVA analysis followed by Tukey multicomparison correction for the means. ns: not statistically significant.

(I) Plot showing analysis of UFBs/cell from the same data. Horizontal bars indicate mean and error bars indicate SD calculated for the means across the independent experiments. p-values indicate one-way ANOVA analysis followed by Tukey multicomparison correction for the means. ns: not statistically significant.

(J–L) GSK-343 treatment in mitosis reduces H3K27me3 at centromeres. (J) An example image of spread chromosomes stained for H3K27me3 (green), CREST (red) and DNA (Hoechst, blue). Bar, 5 μm. Magnified inset shows how mean signal intensity was quantified across centromere regions using a four-pixel wide line tool in ImageJ.

(K) Superplots showing H3K27me3 signal intensity per CREST signal intensity across centromere regions of chromosomes described in panel J.

(L) Superplots showing CREST signal intensity across centromere regions of chromosomes described in panel J, from the same dataset as panel K. DMSO, n = 40 cells and 754 CENs; GSK-343, n = 40 cells, 819 CENs. Data were collected from three experimental repeats (a minimum of 10 cells analyzed per experiment). Horizontal lines show Means and S.D. p-values indicate two-tailed unpaired samples t-test.

αChT and H3K27me3-nucleosomes likely cooperate to prevent UFBs

To explore whether UFBs after GSK-343 treatment are due to a functional relationship between αChT and H3K27me3-nucleosomes, we quantified UFBs in the αChT mutants (Figure 6A). This revealed a correlation between UFBs/cell and the ability of the mutants to bind nucleosomes (Figure 6B). TopoIIα-F1502A and TopoIIα-Y1521A had increased UFBs similar to TopoIIα−ChTΔ and GSK-343/A-196 treated cells. In contrast, TopoIIα−F1531A, which retains significant interaction with mono-nucleosomes, did not show a significant increase in UFBs/cell. This is consistent with the ability of TopoIIα to interact with methylated nucleosomes facilitating decatenation to prevent UFBs. To examine further the possible functional relationship between loss of mono-nucleosome interaction and H3K27me3 modification, we examined the effects of GSK-343 on the TopoIIα mutants (Figures 6C and S10). This revealed a significant increase in UFBs after GSK-343 treatment in TopoIIα-wt and TopoIIα-F1531A cells but no additive increase in TopoIIα-F1502A and TopoIIα-Y1521A mutants that have a deficiency in methylated mono-nucleosome binding. The lack of an additive effect between reducing H3K27me3 (GSK-343 treatment) and reduced mono-nucleosome interaction (αChT mutations) indicates a functional relationship. Altogether, the data provide evidence that αChT interaction with H3K27me3-containing nucleosomes is a mechanism required for complete resolution of the entangled genome that promotes faithful chromosome segregation.

DISCUSSION

Despite having essential and unique roles in mitosis, the molecular basis of how TopoIIα is directed to appropriate substrates to ensure faithful chromosome segregation has been an important but challenging question. Quantification of chromosome segregation errors in the αChT mutant revealed a 2.7-fold increase in aberrant anaphases (Figures 1H–1J). Most of these were chromosome bridges and laggards rather than the complete blockage of chromosome segregation seen after TopoIIα depletion (Figures 1H–1J and S3). These data suggest the crucial role of the αChT is not to promote bulk decatenation of the genome, but to ensure complete resolution of sister centromeres that is essential for high-fidelity chromosome segregation. Indeed, even small numbers of chromosome segregation errors or UFBs give rise to micronuclei that accumulate damaged DNA following cytokinesis.[23] Hence, TopoIIα must resolve each and every catenation because failure results in the accumulation of genomic lesions that contribute to tumorigenesis.[24] How TopoIIα achieves the precision needed to avoid these outcomes was not well understood. The data presented here provides evidence that an interaction between the αChT and specific methylated nucleosomes promotes complete resolution of the genome (Figure 6D).

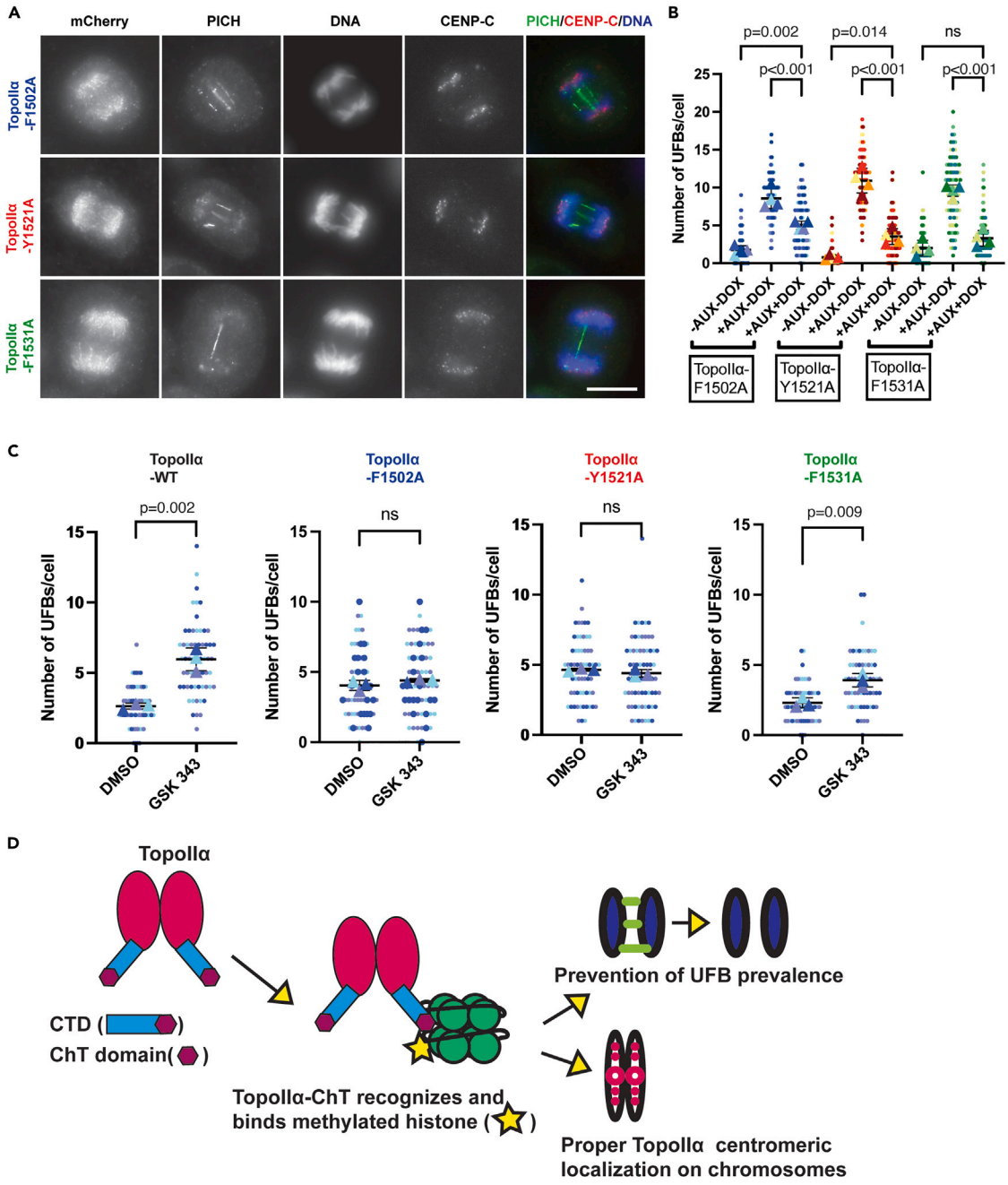

Figure 6. Analysis of UFBs in ChT point mutants and in combination with histone methyl-transferase inhibitor GSK-343

(A) Representative images acquired for UFB quantification after replacement of endogenous TopoIIα with mCherry-TopoIIα ChT point mutants. Cells were synchronized and treated according to the scheme shown in Figure 1E, then stained with anti-PICH antibody to reveal UFBs and CENP-C antibody to mark centromeres. Bars, 10 μm.

(B) Superplots showing quantification of UFBs/cell in the absence of Aux and Dox (i.e., with only endogenous TopoIIα expression), after treatment with Aux only (i.e., after endogenous TopoIIα depletion), or after treatment with Aux and Dox (i.e., with only mCherry-TopoIIα ΔChT point mutant expression) as described in panel A. More than 60 cells were counted over three independent experiments. p-values indicate one-way ANOVA analysis followed by Tukey multicomparison correction for the means. Horizontal bars indicate mean and error bars indicate SD calculated for the means across the three independent experiments. ns: not statistically significant.

(C) Superplots showing quantification of UFBs/cell after GSK-343 treatment was combined with replacement of endogenous TopoIIα for exogenous mCherry-TopoIIα or mCherry-TopoIIα ChT point mutants. Cells were treated as in panel B to replace endogenous TopoIIα (+Aux+Dox) then treated with DMSO or GSK-343 (4 μM) upon release from S-phase synchrony. More than 60 cells were counted over three independent experiments. p-values indicate

Figure 6. *Continued*
one-way ANOVA analysis followed by Tukey multicomparison correction for the means. Horizontal bars indicate mean and error bars indicate SD calculated for the means across the three independent experiments. ns: not statistically significant.
(D) Model describing the mechanism of how the ChT-dependent interaction of TopoIIα with specific methylated nucleosomes may facilitate complete resolution of catenated centromeres in mitosis. TopoIIα recognizes and binds methylated histones on chromatin, particularly H3K27me3 and H4K20me3, dependent on the ChT domain. Evidence supporting a functional relationship between methylation of specific histone residues and decatenation include the lack of an additive effect between GSK-343 and the ChT point mutants in the UFB assay.

At the onset of anaphase, decatenation by TopoIIα is thought to be most prominent at centromeres that remain paired until this crucial cell cycle transition. By precipitating short chromatin fragments containing centromeric CENP-A nucleosomes, Bailey et al. (2016) determined that the adjacent centromeric H3-containing nucleosomes are prominently methylated rather than acetylated.[9] We found the αChT preferentially precipitates mono-nucleosomes with H3K27me3 and H4K20me3. However, the majority of centromeric H4K20 is mono-methylated.[9] Therefore, TopoIIα may only bind a subset of centromeric nucleosomes with H4K20me3. Similarly, centromeric nucleosomes have a complex set of H3 modifications[9] also consistent with TopoIIα binding a subset of specific centromeric sites. Beyond interaction with methylated nucleosomes, there is evidence that the centromeric localization of TopoIIα involves interaction with H2AT120-Phos nucleosomes, because αChT-mediated centromere localization of TopoIIα requires Bub1 kinase that phosphorylates H2AT120.[25] It is intriguing that perturbing any one of these Histone modifications (H3K27me3, H4K20me3 and H2AT120-Phos) increases UFBs, suggesting that proper localization and abundance of TopoIIα at centromeres is critical for ensuring complete resolution of the entangled centromeres at anaphase onset. It will be important to determine if specific nucleosome modifications regulate SPR efficiency at the loci marked by these modifications or if simple enrichment of TopoIIα at centromeres is sufficient to fully decatenate centromeres. The latter seems less likely because there ought to be a molecular mechanism allowing the enzyme to determine where to perform the SPR. Inhibiting the H3K27 methyltransferase during mitosis increased UFBs. Therefore, one speculation is that interaction with specific nucleosomes containing H3K27me3 directs the SPR of TopoIIα toward catenated centromeric DNA. Of interest, inhibition of the H3K27 demethylase also increased UFBs. This might be explained by increased H3K27me3. Because the SPR can either catenate or decatenate substrate DNA molecules, and if H3K27me3 promotes SPR activity, then additional H3K27me3 in the presence of the demethylase inhibitor would be predicted to produce unwanted catenations.

Despite the evidence αChT functionally interacts with methylated nucleosomes to promote decatenation, it remains unclear whether αChT binds directly to methylated histone tails. The strongest evidence is αChT point mutants had differential abilities to bind mono-nucleosomes that correlated with the ability of those mutants to prevent UFBs, and that in those same mutants the incidence of UFBs did not increase on GSK-343 treatment that reduced H3K27 methylation. Even so, it seems likely that TopoIIα binds to nucleosomes with a combination of modifications, including H3K27me3 and H4K20me3, but also with H2AT120-Phos and perhaps other modifications that remain to be explored. The contribution of other histone modifications and/or αChT functions beyond H3K27me3/H4K20me3 interaction could explain the increased defect observed in UFB formation with the ΔChT mutant compared with the aromatic amino acid mutants. The precise molecular interface between specific nucleosomes and TopoIIα needs to be determined by structural approaches for a complete understanding of the regulation of TopoIIα in mitosis via its specific interaction with chromatin. The contribution of αChT binding to specific centromeric nucleosomes in mitosis could go beyond promoting decatenation. In addition to performing the SPR, TopoIIα recruits regulators of mitosis to centromeres. In particular, SUMOylated TopoIIα recruits Haspin kinase, a function conserved in yeast, Xenopus and human.[26–28] In turn, the activity of Haspin at mitotic centromeres provides a binding site for the Chromosome Passenger Complex containing Aurora B kinase.[29] A recent study showed that loss of H4K20me3 reduced Aurora B activity at centromeres.[30] Although this remains to be tested, it is possible that TopoIIα regulates Aurora B recruitment by binding to centromeric nucleosomes containing H4K20me3. It will also be important to test if H3K27me3 contributes to centromeric Aurora B activity.

Limitations of the study

Although we present evidence that complete UFB resolution in mitosis requires mitotic H3K27me3/TopoIIα interaction, there remains a possibility that the mitotic defects observed in the TopoIIα-replaced cell lines originate from defects arising because of loss of TopoIIα function during interphase (because of the limitations of our genetic replacement system). It is possible that TopoIIα function during DNA

replication or during chromosomal structural re-organization after replication contributes to chromosome bridge formation in anaphase. As we indicated in the Discussion section, we were not able to provide the structural basis of TopoIIα-ChT interaction with methylated histone containing nucleosomes because of lack of structural information about the TopoIIα-CTD. The structural/biochemical basis of the TopoIIα interaction with specific chromatin is an important future interest. Use of chemical inhibitors of the histone methyltransferase/demethylase enzymes is subject to the possibility of off-target effects that cannot be anticipated. It will be an important future goal to investigate the dynamics of histone methylation during mitosis after genetically manipulating the methyltransferase/demethylase activities in live cells.

STAR★METHODS

Detailed methods are provided in the online version of this paper and include the following:

- KEY RESOURCES TABLE
- RESOURCE AVAILABILITY
  - Lead contact
  - Materials availability
  - Data and code availability
- EXPERIMENTAL MODEL AND SUBJECT DETAILS
  - Human cell lines
- METHOD DETAILS
  - DNA constructs, recombinant proteins, and antibodies preparation
  - Cell culture and transfections
  - Preparation of whole cell lysate and mitotic chromosome samples
  - Western blotting
  - UFB assays, immunostaining, and live cell imaging
  - Morphological quantification of TopoII distribution with wndchrm
  - Mono-nucleosome pull-down assays
  - Methyl transferase inhibitor addition conditions and assays with inhibitor treatment
- QUANTIFICATION AND STATISTICAL ANALYSIS

SUPPLEMENTAL INFORMATION

Supplemental information can be found online at https://doi.org/10.1016/j.isci.2023.106743.

ACKNOWLEDGMENTS

This work was supported by NIH/NIGMS, GM112793 and GM130858, then in part, by NIH/NCIR 21CA259718 and KUCC/CB pilot grant (KAN1000623) and General research funds from University of Kansas (#2144098 and #2144083). It was also supported by JSPS KAKENHI Grant Numbers JP18H05531, JP18K19310, JP20H03520 [to N.S.], and by grants from The Vehicle Racing Commemorative Foundation [to N.S.]. A. Arnaoutov and M. Dasso are supported by NIH/NICHD Intramural projects Z01 HD008954 and ZIA HD001902.

AUTHOR CONTRIBUTIONS

SS conducted chromatin pull-down assays, created TopoII mutant replaced cell lines in Figure 3, performed UFB assay with them, optimized GSK-343 treatment conditions and performed cell-based assays in Figures 2, 5, and 6, and drafted the manuscript. HP created AID-TopoIIα cell lines and most of the TopoII mutant replaced lines, performed cell-based assays in Figures 1, 2, and S4, and acquired images. BL performed part of pull-down assays in Figures 1C and 3C, and confirmed genome editing of the cells by gPCR and western blotting for Figures S2D and S5, and part of UFB assays in Figure 5. SK established AID-TopoII line then performed initial UFB assay in Figure 5 for TopoIIα-depleted cells. DC co-designed study with YA and performed live cell imaging and analysis together with MJ and DK. TF and NS performed wndchrm analysis of the images in Figure 4. AA and MD provided original gene targeting plasmids for OsTIR and CENP-A. ZW synthesized GSK-J4 and provided important insight regarding its use in live cells. YA designed the study, supervised project, and co-wrote the manuscript with DC.

DECLARATION OF INTERESTS

The authors declare no competing financial interests.

INCLUSION AND DIVERSITY

We support inclusive, diverse, and equitable conduct of research.

Received: August 16, 2022
Revised: October 31, 2022
Accepted: April 21, 2023
Published: April 25, 2023

REFERENCES

1. Nitiss, J.L. (2009). Targeting DNA topoisomerase II in cancer chemotherapy. Nat. Rev. Cancer *9*, 338–350. https://doi.org/10.1038/nrc2607.

2. Gilroy, K.L., and Austin, C.A. (2011). The impact of the C-terminal domain on the interaction of human DNA topoisomerase II alpha and beta with DNA. PLoS One *6*, e14693. https://doi.org/10.1371/journal.pone.0014693.

3. Grue, P., Grässer, A., Sehested, M., Jensen, P.B., Uhse, A., Straub, T., Ness, W., and Boege, F. (1998). Essential mitotic functions of DNA topoisomerase IIalpha are not adopted by topoisomerase IIbeta in human H69 cells. J. Biol. Chem. *273*, 33660–33666. https://doi.org/10.1074/jbc.273.50.33660.

4. Linka, R.M., Porter, A.C.G., Volkov, A., Mielke, C., Boege, F., and Christensen, M.O. (2007). C-terminal regions of topoisomerase IIalpha and IIbeta determine isoform-specific functioning of the enzymes in vivo. Nucleic Acids Res. *35*, 3810–3822. https://doi.org/10.1093/nar/gkm102.

5. Sakaguchi, A., and Kikuchi, A. (2004). Functional compatibility between isoform alpha and beta of type II DNA topoisomerase. J. Cell Sci. *117*, 1047–1054. https://doi.org/10.1242/jcs.00977.

6. Choppakatla, P., Dekker, B., Cutts, E.E., Vannini, A., Dekker, J., and Funabiki, H. (2021). Linker histone H1.8 inhibits chromatin binding of condensins and DNA topoisomerase II to tune chromosome length and individualization. Elife *10*, e68918. https://doi.org/10.7554/eLife.68918.

7. Shintomi, K., and Hirano, T. (2021). Guiding functions of the C-terminal domain of topoisomerase IIalpha advance mitotic chromosome assembly. Nat. Commun. *12*, 2917. https://doi.org/10.1038/s41467-021-23205-w.

8. Lane, A.B., Giménez-Abián, J.F., and Clarke, D.J. (2013). A novel chromatin tether domain controls topoisomerase IIalpha dynamics and mitotic chromosome formation. J. Cell Biol. *203*, 471–486. https://doi.org/10.1083/jcb.201303045.

9. Bailey, A.O., Panchenko, T., Shabanowitz, J., Lehman, S.M., Bai, D.L., Hunt, D.F., Black, B.E., and Foltz, D.R. (2016). Identification of the post-translational modifications present in centromeric chromatin. Mol. Cell. Proteomics *15*, 918–931. https://doi.org/10.1074/mcp.M115.053710.

10. Hassebroek, V.A., Park, H., Pandey, N., Lerbakken, B.T., Aksenova, V., Arnaoutov, A., Dasso, M., and Azuma, Y. (2020). PICH regulates the abundance and localization of SUMOylated proteins on mitotic chromosomes. Mol. Biol. Cell *31*, 2537–2556. https://doi.org/10.1091/mbc.E20-03-0180.

11. Nielsen, C.F., Zhang, T., Barisic, M., Kalitsis, P., and Hudson, D.F. (2020). Topoisomerase IIalpha is essential for maintenance of mitotic chromosome structure. Proc. Natl. Acad. Sci. USA *117*, 12131–12142. https://doi.org/10.1073/pnas.2001760117.

12. Tavormina, P.A., Côme, M.G., Hudson, J.R., Mo, Y.Y., Beck, W.T., and Gorbsky, G.J. (2002). Rapid exchange of mammalian topoisomerase II alpha at kinetochores and chromosome arms in mitosis. J. Cell Biol. *158*, 23–29. https://doi.org/10.1083/jcb.200202053.

13. Verma, S.K., Tian, X., LaFrance, L.V., Duquenne, C., Suarez, D.P., Newlander, K.A., Romeril, S.P., Burgess, J.L., Grant, S.W., Brackley, J.A., et al. (2012). Identification of potent, selective, cell-active inhibitors of the histone lysine methyltransferase EZH2. ACS Med. Chem. Lett. *3*, 1091–1096. https://doi.org/10.1021/ml3003346.

14. Bromberg, K.D., Mitchell, T.R.H., Upadhyay, A.K., Jakob, C.G., Jhala, M.A., Comess, K.M., Lasko, L.M., Li, C., Tuzon, C.T., Dai, Y., et al. (2017). The SUV4-20 inhibitor A-196 verifies a role for epigenetics in genomic integrity. Nat. Chem. Biol. *13*, 317–324. https://doi.org/10.1038/nchembio.2282.

15. Jacobs, S.A., and Khorasanizadeh, S. (2002). Structure of HP1 chromodomain bound to a lysine 9-methylated histone H3 tail. Science *295*, 2080–2083. https://doi.org/10.1126/science.1069473.

16. Min, J., Zhang, Y., and Xu, R.M. (2003). Structural basis for specific binding of Polycomb chromodomain to histone H3 methylated at Lys 27. Genes Dev. *17*, 1823–1828. https://doi.org/10.1101/gad.269603.

17. Nielsen, P.R., Nietlispach, D., Mott, H.R., Callaghan, J., Bannister, A., Kouzarides, T., Murzin, A.G., Murzina, N.V., and Laue, E.D. (2002). Structure of the HP1 chromodomain bound to histone H3 methylated at lysine 9. Nature *416*, 103–107. https://doi.org/10.1038/nature722.

18. Shamir, L., Orlov, N., Eckley, D.M., Macura, T., Johnston, J., and Goldberg, I.G. (2008). Wndchrm - an open source utility for biological image analysis. Source Code Biol. Med. *3*, 13. https://doi.org/10.1186/1751-0473-3-13.

19. Biebricher, A., Hirano, S., Enzlin, J.H., Wiechens, N., Streicher, W.W., Huttner, D., Wang, L.H.C., Nigg, E.A., Owen-Hughes, T., Liu, Y., et al. (2013). PICH: a DNA translocase specially adapted for processing anaphase bridge DNA. Mol. Cell *51*, 691–701. https://doi.org/10.1016/j.molcel.2013.07.016.

20. Gemble, S., and Amor-Guéret, M. (2021). Identification and analysis of different types of UFBs. Methods Mol. Biol. *2153*, 187–192. https://doi.org/10.1007/978-1-0716-0644-5_13.

21. Moreno, A., Carrington, J.T., Albergante, L., Al Mamun, M., Haagensen, E.J., Komseli, E.S., Gorgoulis, V.G., Newman, T.J., and Blow, J.J. (2016). Unreplicated DNA remaining from unperturbed S phases passes through mitosis for resolution in daughter cells. Proc. Natl. Acad. Sci. USA *113*, E5757–E5764. https://doi.org/10.1073/pnas.1603252113.

22. Kruidenier, L., Chung, C.W., Cheng, Z., Liddle, J., Che, K., Joberty, G., Bantscheff, M., Bountra, C., Bridges, A., Diallo, H., et al. (2012). A selective jumonji H3K27 demethylase inhibitor modulates the proinflammatory macrophage response. Nature *488*, 404–408. https://doi.org/10.1038/nature11262.

23. Hengeveld, R.C.C., de Boer, H.R., Schoonen, P.M., de Vries, E.G.E., Lens, S.M.A., and van Vugt, M.A. (2015). Rif1 is required for resolution of ultrafine DNA bridges in anaphase to ensure genomic stability. Dev. Cell *34*, 466–474. https://doi.org/10.1016/j.devcel.2015.06.014.

24. Krupina, K., Goginashvili, A., and Cleveland, D.W. (2021). Causes and consequences of micronuclei. Curr. Opin. Cell Biol. *70*, 91–99. https://doi.org/10.1016/j.ceb.2021.01.004.

25. Zhang, M., Liang, C., Chen, Q., Yan, H., Xu, J., Zhao, H., Yuan, X., Liu, J., Lin, S., Lu, W., and Wang, F. (2020). Histone H2A phosphorylation recruits topoisomerase IIalpha to centromeres to safeguard genomic stability. EMBO J. *39*, e101863. https://doi.org/10.15252/embj.2019101863.

26. Edgerton, H., Johansson, M., Keifenheim, D., Mukherjee, S., Chacón, J.M., Bachant, J., Gardner, M.K., and Clarke, D.J. (2016). A noncatalytic function of the topoisomerase II CTD in Aurora B recruitment to inner centromeres during mitosis. J. Cell Biol. *213*, 651–664. https://doi.org/10.1083/jcb.201511080.

27. Pandey, N., Keifenheim, D., Yoshida, M.M., Hassebroek, V.A., Soroka, C., Azuma, Y., and Clarke, D.J. (2020). Topoisomerase II SUMOylation activates a metaphase checkpoint via Haspin and Aurora B kinases. J. Cell Biol. *219*, e201807189. https://doi.org/10.1083/jcb.201807189.

28. Yoshida, M.M., Ting, L., Gygi, S.P., and Azuma, Y. (2016). SUMOylation of DNA topoisomerase IIalpha regulates histone H3 kinase Haspin and H3 phosphorylation in mitosis. J. Cell Biol. *213*, 665–678. https://doi.org/10.1083/jcb.201511079.

29. Wang, F., Dai, J., Daum, J.R., Niedzialkowska, E., Banerjee, B., Stukenberg, P.T., Gorbsky, G.J., and Higgins, J.M.G. (2010). Histone H3 Thr-3 phosphorylation by Haspin positions Aurora B at centromeres in mitosis. Science *330*, 231–235. https://doi.org/10.1126/science.1189435.

30. Herlihy, C.P., Hahn, S., Hermance, N.M., Crowley, E.A., and Manning, A.L. (2021). Suv420 enrichment at the centromere limits Aurora B localization and function. J. Cell Sci. *134*, jcs249763. https://doi.org/10.1242/jcs.249763.

31. Concordet, J.P., and Haeussler, M. (2018). CRISPOR: intuitive guide selection for CRISPR/Cas9 genome editing experiments and screens. Nucleic Acids Res. *46*, W242–W245. https://doi.org/10.1093/nar/gky354.

32. Natsume, T., Kiyomitsu, T., Saga, Y., and Kanemaki, M.T. (2016). Rapid protein depletion in human cells by auxin-inducible degron tagging with short homology donors. Cell Rep. *15*, 210–218. https://doi.org/10.1016/j.celrep.2016.03.001.

33. Ryu, H., Al-Ani, G., Deckert, K., Kirkpatrick, D., Gygi, S.P., Dasso, M., and Azuma, Y. (2010). PIASy mediates SUMO-2/3 conjugation of poly(ADP-ribose) polymerase 1 (PARP1) on mitotic chromosomes. J. Biol. Chem. *285*, 14415–14423. https://doi.org/10.1074/jbc.M109.074583.

34. Zhu, F., Gamboa, M., Farruggio, A.P., Hippenmeyer, S., Tasic, B., Schüle, B., Chen-Tsai, Y., and Calos, M.P. (2014). DICE, an efficient system for iterative genomic editing in human pluripotent stem cells. Nucleic Acids Res. *42*, e34. https://doi.org/10.1093/nar/gkt1290.

35. Baumann, C., Körner, R., Hofmann, K., and Nigg, E.A. (2007). PICH, a centromere-associated SNF2 family ATPase, is regulated by Plk1 and required for the spindle checkpoint. Cell *128*, 101–114. https://doi.org/10.1016/j.cell.2006.11.041.

36. Ke, Y., Huh, J.W., Warrington, R., Li, B., Wu, N., Leng, M., Zhang, J., Ball, H.L., Li, B., and Yu, H. (2011). PICH and BLM limit histone association with anaphase centromeric DNA threads and promote their resolution. EMBO J. *30*, 3309–3321. https://doi.org/10.1038/emboj.2011.226.

37. Spence, J.M., Phua, H.H., Mills, W., Carpenter, A.J., Porter, A.C.G., and Farr, C.J. (2007). Depletion of topoisomerase IIalpha leads to shortening of the metaphase interkinetochore distance and abnormal persistence of PICH-coated anaphase threads. J. Cell Sci. *120*, 3952–3964. https://doi.org/10.1242/jcs.013730.

38. Matsumoto, A., Sakamoto, C., Matsumori, H., Katahira, J., Yasuda, Y., Yoshidome, K., Tsujimoto, M., Goldberg, I.G., Matsuura, N., Nakao, M., et al. (2016). Loss of the integral nuclear envelope protein SUN1 induces alteration of nucleoli. Nucleus *7*, 68–83. https://doi.org/10.1080/19491034.2016.1149664.

39. Ono, T., Sakamoto, C., Nakao, M., Saitoh, N., and Hirano, T. (2017). Condensin II plays an essential role in reversible assembly of mitotic chromosomes in situ. Mol. Biol. Cell *28*, 2875–2886. https://doi.org/10.1091/mbc.E17-04-0252.

40. Takagi, M., Ono, T., Natsume, T., Sakamoto, C., Nakao, M., Saitoh, N., Kanemaki, M.T., Hirano, T., and Imamoto, N. (2018). Ki-67 and condensins support the integrity of mitotic chromosomes through distinct mechanisms. J. Cell Sci. *131*, jcs212092. https://doi.org/10.1242/jcs.212092.

41. Tokunaga, K., Saitoh, N., Goldberg, I.G., Sakamoto, C., Yasuda, Y., Yoshida, Y., Yamanaka, S., and Nakao, M. (2014). Computational image analysis of colony and nuclear morphology to evaluate human induced pluripotent stem cells. Sci. Rep. *4*, 6996. https://doi.org/10.1038/srep06996.

42. Johnston, J., Iser, W.B., Chow, D.K., Goldberg, I.G., and Wolkow, C.A. (2008). Quantitative image analysis reveals distinct structural transitions during aging in Caenorhabditis elegans tissues. PLoS One *3*, e2821. https://doi.org/10.1371/journal.pone.0002821.

43. Felsenstein, J. (1989). PHYLIP—phylogeny inference package (version 3.2). Cladistics *5*, 164–166.

STAR★METHODS

KEY RESOURCES TABLE

REAGENT or RESOURCE	SOURCE	IDENTIFIER
Antibodies		
Mouse anti-FlAG M2	Millipore/SIgma	Cat# F1804 RRID:AB_262044
Rat anti-DYKDDDDK	Agilent	Cat# 200474 RRID:AB_10597743
Rabbit anti-mCherry	Abcam	Cat #ab167453 RRID:AB_2571870
Mouse anti-HIstone H4	Active Motif	Cat #61521 RRID:AB_2793667
Mouse anti-β-tubulin	Millipore/SIgma	Cat #T-4026 RRID:AB_477577
Mouse anti-Histone H4K20me3	Active Motif	Cat #39671 RRID:AB_2650526
Rabbit anti-Histone H3K27me2	abcam	Cat #ab24684 RRID:AB_448222
Rabbit anti-Histone H3K27me3	Cell Signaling Technology	Cat #9733 RRID:AB_2616029
Mouse anti-Histone H3K27me3	Active Motif	Cat #61018 RRID:AB_2614987
Mouse anti-Histone H3	Cell Signaling Technology	Cat #3638 RRID:AB_1642229
Mouse anti-Histone H3K9me3	Active Motif	Cat #61013 RRID:AB_2687870
Mouse anti-Histone H3K4me3	Active Motif	Cat #61379 RRID:AB_2793611
Rabbit anti-Phspho Histone H3 Ser28	Cell Signaling Technology	Cat #9713 RRID:AB_823532
Rabbit anti-Histone H2A	Cell Signaling Technology	Cat #12349 RRID:AB_2687875
Mouse anti-Histone H2B	Cell Signaling Technology	Cat #2934 RRID:AB_2295301
Guinea pig anti-CENP-C	MBL International	Cat# PD030, RRID:AB_10693556
Rabbit anti-Histone H3K27me3	Millipore (Upstate)	Cat# 07-449 RRID:AB_310624
Rat anti-RFP	ChromoTek/Bulldog Bio	Cat# 5f8(RMA5F8) RRID:AB_2336064
CREST serum	Cortex Biochem	CS1058, RRID:AB_1282595
Goat anti-Rabbit IgG Alexa Fluor 488	Thermo Fisher Scientific	Cat# A-11034, RRID:AB_2576217
Goat anti-Rat IgG Alexa Fluor 568	Thermo Fisher Scientific	Cat# A-11077 RRID:AB_2534121
Goat anti-Guinea Pig IgG Alexa Fluor 647	Thermo Fisher Scientific	Cat# A-21450, RRID:AB_2735091
IRDye®800CW Goat anti-Rabbit IgG	LI-COR Biosciences	Cat# 926-32211, RRID:AB_621843
IRDye 800CW Goat anti-Mouse IgG	LI-COR Biosciences	Cat# 926-32210, RRID:AB_621842
IRDye 680RD Goat anti-Rabbit IgG	LI-COR Biosciences	Cat# 926-68071, RRID:AB_10956166
IRDye 680RD Goat anti-Mouse IgG	LI-COR Biosciences	Cat# 926-68070, RRID:AB_10956588
Rabbit anti-human Top2A	in house	N/A
Rabbit anti-human PICH	in house	N/A
Rabbit anti-SUMO2/3	in house	N/A
Bacterial and virus strains		
Rosetta 2(DE3)	Novagen (Millipore/Sigma)	Cat# 71397
NEB®5-alpha	New England BioLabs	Cat# C2987
NEB®Turbo	New England BioLabs	Cat# C2984
Chemicals, peptides, and recombinant proteins		
GSK-343	APExBIO	Cat# A3449
A-193	Cayman chemical	Cat# 18317
S-protin HRP cojugate	Millipore/Sigma	Cat# 69047
Viafect	Promega	Cat# E4981
S-protein Agarose	Millipore/Sigma	Cat# 69704
Doxycycline Hydrochloride	Millipore/Sigma	Cat# D3072

(*Continued on next page*)

Continued

REAGENT or RESOURCE	SOURCE	IDENTIFIER
Indole-3-acetic acid (Auxin)	Millipore/Sigma	Cat# I5148
Critical commercial assays		
QuikChange II XL Site-Directed Mutagenesis Kit	Agilent	Cat# 200521
Experimental models: Cell lines		
Human DLD-1	ATCC	Cat# CCL-221
Oligonucleotides		
See Table S1 for oligo DNA sequences	IDT	N/A
Recombinant DNA		
pX330-U6-Chimeric_BB-CBh-hSpCas9	Addgene	#42230
Software and algorithms		
CRISPR design tools	Zhang laboratory, MIT http://crispr.mit.edu:8079	N/A
CRISPOR	http://crispor.tefor.net	N/A
wndchrm	https://github.com/wnd-charm/wnd-charm	N/A
Fiji/ImageJ	https://inagej.net/Contributors	N/A
Image Studio Version 5.2	LI-COR	N/A
Prism	GraphPad	N/A

RESOURCE AVAILABILITY

Lead contact

Further information and requests for resources and reagents should be directed to and will be fulfilled by the lead contact, Dr. Yoshiaki Azuma (azumay@ku.edu).

Materials availability

The plasmids and cell lines generated in this study were not deposited to repositories. However, all plasmids and cell lines that were used in this study will be made available through requests submitted to the lead contact.

Data and code availability

- All data reported in this paper will be shared by the lead contact upon request.
- This paper does not report original code.
- Any additional information required to reanalyze the data reported in this paper is available from the lead contact upon request.

EXPERIMENTAL MODEL AND SUBJECT DETAILS

Human cell lines

DLD1 colon cancer cells originally obtained from ATCC were used in this study. The cells were grown in 1X McCoy's 5A 1X Glutamine 7.5% Fetal Bovine Serum (FBS) media for no more than 10 passages. They were maintained at 37°C and 5% CO_2. All our genetically engineered cell lines were validated by genomic PCR to ensure correct insertion of the transgene prior to their use in experiments.

METHOD DETAILS

DNA constructs, recombinant proteins, and antibodies preparation

The donor plasmid for OsTIR1 targeting was made by inserting OsTIR sequence fused with Blasticidin resistant gene via P2A sequence into between homology arm sequences for 3'end of RCC1 locus.[10] The plasmid for AID-TopoIIα tagging was created by inserting AID-3xFLAG sequence fused to Hygromycin resistant

gene into between homology arm sequences of 5′ end of TopoIIα locus.[10] The mNeon fusion donor for endogenous TopoIIα and PICH were created by replacing AID sequence to mNeon sequence of TopoIIα or PICH N-terminal targeting donor plasmids.[10] In this study, the donor plasmids for miRFP670 fusion to endogenous CENP-A at its C-terminal was created. The homology arms for CENP-A C-terminal were amplified using primers listed in supplemental information (Table S1) from genomic DNA of DLD-1 cells. The amplified CENP-A homology arms were inserted into the plasmid by using PciI/SalI and SpeI/NotI sites in the C-terminal targeting donor plasmid carrying miRFP670 fused to Puromycin resistant gene via T2A sequence as shown in Figure S5. The guide RNA sequences for CENP-A C-terminal targeting are listed in supplemental information (Table S1) were designed using CRISPR design tools from http://crispr.mit.edu:8079 (Zhang laboratory, MIT) or CRISPOR.[31] The synthesized oligo DNA primers for the guides were inserted into pX330 (Addgene #42230). For Tet-inducible expression of exogenous TopoII, TopoII cDNAs fused with mCherry at their N-terminus were inserted into MluI/SalI site on the hH11 Tet-ON cassette[32] donor plasmid described previously.[10] cDNA fragments of TopoIIα and TopoIIβ CTD were amplified from full length cDNA and then cloned in the pET30a plasmid (EMD Millipore/Novagen). The TopoIIα truncation mutants were generated using PCR, and the point mutations were generated using site-directed mutagenesis by a QuikChangeII kit (Agilent) with the primers listed in supplemental information (Table S1). All constructs were verified by DNA sequencing. The parental line construct for OsTIR1 targeting and the TopoIIα-AID construct were created as described previously.[10]

For preparation of recombinant TopoII-CTD proteins, the proteins were expressed in Rossetta2 (DE3) strain culture in 2xYT media containing 5% Glycerol with 0.2 mM IPTG at 15°C.[33] The bacterial pellet was harvested the following day and the cells were lysed using lysozyme in Lysis Buffer (450 mM NaCl, 30 mM HEPES (pH 7.7), 0.5 mM TCEP). After incubation at 4°C for 1h, 5% Glycerol, 1% Triton X-100, 10 units/ml DNase1,10 mM $MgCl_2$, 0.1 mM PMSF and 0.5 mM TCEP were added, and the suspension was incubated again for 1h at 4°C. The suspension was then centrifuged at 12000 rpmat 4°C for 30 min. His6-tagged protein in the supernatant was captured on Talon Sepharose beads (#635502, Clontech/Takara) pre-equilibrated against Buffer1 (300 mM NaCl, 20 mM HEPES (pH 7.7), 2 mM $MgCl_2$, 2.5 mM Imidazole and 0.5 mM TCEP). After incubation with Talon beads at 4°C for 1-2h, the beads bound with protein were emptied into a column, the column was washed with 5 volumes of Buffer1 containing 2.5 mM ATP, 5 mM $MgCl_2$ and 2.5 mM Imidazole and 0.5 mM TCEP and 2 volumes of Buffer2 (50 mM NaCl, 10 mM HEPES (pH 7.7) and 2 mM $MgCl_2$) containing 2.5mM Imidazole and 0.5mM TCEP. Elution was then carried out using 15 mM, 75 mM, and 450 mM Imidazole in Buffer 2. The eluted fractions were then tested using SDS-PAGE followed by CBB staining. The fractions that contained the protein were pooled and subjected to Hi-trap ionexchange chromatography (GE healthcare) for further purification.

The α-PICH and α-TopoIIα antibodies were generated as previously described.[10]

Cell culture and transfections

CRISPR/Cas9 targeted insertion was performed as previously described to generate all the cell lines.[10] In brief, DLD-1 cells were transfected with the guide and donor plasmids using Viafect (#E4981, Promega) reagent. Transfections were set up in 3.5 cm dishes. 2 days after, the cells were trypsinized and replated on a 10cm dish at ≈20% confluency and starting from Day 3, they were subjected to a selection process by maintaining them in the presence of a suitable selection reagent (1μg/ml Blasticidin [#ant-bl, Invivogen], 0.5μg/ml Puromycin [#ant-pr, Invivogen], 200μg/ml Hygromycin B gold [#ant-hg, Invivogen]). After 10-14 days of this process, the colonies were isolated and cultured in 48-well plates. The colonies were subjected to Western Blotting and Genomic PCR analyses to verify the integration of the transgene. For Western Blotting analyses, the cells were pelleted and boiled/vortexed with 1X SDS-PAGE sample buffer. The samples were analyzed using antibodies as described in each Figure legend.

Genomic DNA was isolated by cell pelleting and lysis using lysis buffer (100 mM Tris-HCl (pH 8.0), 200 mM NaCl, 5 mM EDTA, 1% SDS, and 0.6 mg/ml proteinase K [#P8107S, NEB]) followed by Ethanol precipitation and resuspension with TE buffer containing 50 μg/mlRNase A (#EN0531, ThermoFisher). The obtained genomic DNA samples were subjected to PCR using primers indicated in the supplemental information to ensure integration at the correct locus.

The specific gene targeted cell lines were established using the OsTIR1 parental DLD-1 line.[10] The targeting donor plasmids and pX330 guide plasmids were transfected as above to isolate candidate clones. The

candidate clones obtained were screened by genomic PCR to verify accurate transgene integration. Once validated for integration, the ability of Aux to deplete the protein was tested by Western blotting and Immunostaining. For fluorescent fusion, clones were verified by Western blotting by increased molecular weight and fluorescent signal for desired fluorescence by fluorescent microscope analysis. The mCherry-TopoII wt or mutant replacement cell lines were also engineered using CRISPR/Cas9 in the TopoIIα-AID cell line by inserting the gene coding for the rescue candidate at the hH11 locus,[34] as previously described[10] and as indicated in the supplemental information. The isolated clones were validated for transgene integration using genomic PCR analysis. The expression of the mCherry-fusion protein was confirmed using Western Blotupon addition of Dox. The CENP-A-miRFP670/mNeon-TopoIIα line was created using OsTIR/AID-PICH line,[10] then validated as shown in Figure S5 with genomic PCR.

Preparation of whole cell lysate and mitotic chromosome samples

For preparation of the whole cell lysate for testing most of AID system-based degradation, cells were synchronized with Thymidine for 18-24h. Upon release, the cells were replenished with media containing 0.5 mM Aux to allow degradation of endogenous AID-tagged proteins. After ≈8.5 hours, the cells were harvested and boiled/vortexed with 1X SDS-PAGE sample buffer and subjected to Western Blotting with antibodies as indicated in the Figure legends. For preparation of mitotic chromosomes from the cell lines, a mitotic shake-off was performed. For this, the cells were plated and at ≈ 70% confluency, they were treated with Thymidine. After 18 hours, the cells were released from Thymidine for 6 hours following which they were treated with Nocodazole (100ng/ml) for 4 hours. The mitotic cells were then detached from the plate, washed using 1X McCoy's devoid of FBS, three times, and resuspended in fresh 1X McCoy's media containing FBS for releasing them from Nocodazole for 30 minutes. PostNocodazole release, the cells were pelleted and incubated on ice for 5 minutes with lysis buffer (250 mM sucrose, 20 mM HEPES (pH 7.7), 100 mM NaCl, 1.5 mM $MgCl_2$, 1 mM EDTA, 1 mM EGTA, 0.2% Triton X-100, 1:2000 LPC [leupeptin, pepstatin, chymostatin; 20 mg each/ml in DMSO; Sigma-Aldrich], and 20 mM iodoacetamide [Sigma-Aldrich #I1149]). Chromosomes were isolated from the lysed cells by loading the lysate on to 40% glycerol cushion and centrifuging at 3000 rpm for 5 minutes at 4°C. After washing with 40% glycerol cushion, the isolated chromosomes were boiled and vortexed with 1X SDS-PAGE sample buffer and subjected to Western Blotting.

The whole cell lysates for verifying induction of the mCherry-fusion protein with Dox were prepared by synchronizing cells with Thymidine (-Aux/+Aux/+Aux+Dox samples were all consistently prepared). Upon release from Thymidine block, the cells were concurrently treated with 0.5 mM Aux and 100 μg/ml Dox to allow degradation of endogenous TopoIIα with the simultaneous expression of the rescue candidate, ≈8.5 hours after which the cells were harvested and subjected to Western Blotting as specified in the above two scenarios.

The primary antibodies used were α-TopoIIα (in-house), α-PICH (in-house), α-FLAG M2 (#F1804, Millipore/Sigma), α-mCherry (#ab167453, Abcam), α-H4 (#61521, Active Motif), α-H4K20me3 (#39671, Active Motif) and β-tubulin (#T-4026, Sigma). β-tubulin was used as the loading control for whole cell lysate samples and α-H4 was used in the case of Chromosome samples.

Western blotting

The samples for SDS-PAGE were loaded and separated on handmade/gradient (Invitrogen/ThermoFisher scientific) gels followed by transfer on to a methanol activated PVDF membrane using an ECL-semidry transfer unit (Amersham Biosciences). Following blocking using casein or hydrolyzed gelatin, the proteins of interest were selectively probed for, using primary antibodies as indicated in each Figure legend. The secondary antibodies used were IRDye 800CW secondary antibodies and IRDye 680 RD antibodies (LICOR). Signals were visualized using the LI-COR Odyssey Fc machine.

UFB assays, immunostaining, and live cell imaging

DLD-1 cells were grown for no longer than 10 passages in McCoy's 5A 1X L-Glutamine containing 7.5% Fetal Bovine serum (FBS). Cells were plated on coverslips coated with Poly-D-Lysine (#A38904-01, gibco/Life Technologies Corporation) in a 3.5 cm dish. The coating was done by incubating the flame sterilized coverslips in Poly-D-Lysine solution for >1h. The coat was then removed, and the coverslips were allowed to dry for >3h. Cells were incubated with 2 mM Thymidine (added at ≈ 70% confluency) for 18-24h for synchronization. Thymidine was washed off using McCoy's media lacking FBS, three times. After washing

off Thymidine, 0.5mM Aux and 1μg/ml Dox were added to media containing FBS and the cells were incubated in the same to allow release from the Thymidine treatment. ≈8.5 hours post-release, a major fraction of cells "roundup". At this point, the cells were fixed and stained using suitable antibodies. Fixation was performed using a 4% solution of paraformaldehyde (pFA) in 1X PBS for 10 minutes. After washing off the pFA, the cells were permeabilized using methanol at -20°C for 10 minutes. The cells were then blocked with a 2.5% solution of hydrolyzed gelatin prepared in 1X PBS for 1 hour. Following this, the cells were incubated with a cocktail of primary antibodies for 3 hours to overnight, washed with 1X PBS-T for 10 -minutes, thrice, and then treated with secondary antibodies for 1h before being washed and mounted onto slide glasses with VECTASHIELD Antifade Mounting Medium containing 4′,6-diamidino-2-phenylindole (#H-1200, Vector Laboratory) and sealed using nail polish.

For scoring the UFB phenotype after PICH immuno-staining, we focused on anaphase cells at a consistent stage by ensuring that the CENP-C signals between the segregating chromosomes were at a similar distance, as well as after making sure that the DAPI signals were well distinguishable between segregating chromosomes. Cells which had progressed to anaphase-B were excluded from the counting procedure. PICH staining was used as a readout for UFBs as PICH localizes to these structures.[35–37] All the UFBs that can be visualized were counted by switching the plane of imaging. The UFB number for each of the cells was recorded. For each cell line represented in this study, the UFB number was obtained from a minimum of 60 cells visualized across three independent experiments with at least 20 cells being counted from each experiment. For live cell analysis of UFBs, cells were used with both endogenous PICH alleles tagged with mNeon (Figure S5). After a 30-min accumulation of mitotic cells with colcemid, inhibitors of methyltransferase/demethylase inhibitors (GSK-343; 15 μM, or GSK-J4; 5μM) were added and cells incubated for 90 minutes before releasing from the arrest with the inhibitors only, at which point live cell imaging was started on the DeltaVision Ultra microscope (5 min.intervals, 22μm z-sections with 1μm spacing). Images were processed by deconvolution and quick projection before UFBs were counted in anaphase cells selected according to the criteria above.

The stained cell images were acquired using the Plan Apo 100x/1.4 objective lens on a Nikon TE2000-U equipped PRIME-BSI CMOS camera (Photometrics) with MetaMorph imaging software. Figures were prepared from exported images by adjusting the intensity with ImageJ software, following the guidelines of the Journal.

For quantification of TopoIIα on mitotic chromosomes in live cells, endogenous TopoIIα was depleted, and mCherry-tagged alleles were induced as described above. To ensure cells were at an equivalent stage of mitosis, Nocodazole was added 20 minutes before imaging. Then, mCherry in live cells was imaged under normal cell culture conditions, at 37°C and 5% CO_2, with Nocodazole, using a DeltaVision Ultra microscope fitted with an Olympus 60X/1.42, Plan Apo N objective (UIS2, 1-U2B933), C-Y-R Polychroic, and PCO-Edge sCMOS camera (>82% QE), using the following acquisition parameters. Entire mitotic cell volumes were obtained by capturing 24μm thick Z-series with 0.2μm spacing, i.e., 120 slices per cell. 50ms exposure and 10% lamp power resulted in a rapid Z-series capture time of approximately 6 seconds, which limited image distortion that would have resulted from chromosome movements. Z-series were cropped above and below the cell then projected using SoftWoRx software, then mCherry signal was quantified using ImageJ software by averaging the signal intensities across a 50-pixel wide line spanning the chromosomes.

For quantification of H3K27me3 at mitotic centromeres, cells were treated with colcemid for 30 minutes to accumulate mitotic cells, then DMSO or methyltransferase inhibitor GSK-343 (15μM) was added for 90 minutes before processing for Immuno-Staining, as follows. The mitotic cells were washed with PBS, incubated at room temperature for 5 minutes in a hypotonic solution (50% PBS, 50% dH_20), spun onto glass slides using a Cytospin, fixed immediately for 5 minutes with PFA followed by a 2 minute incubation with Methanol at -20°C. The antibodies used for staining are specified below. A DeltaVision Ultra microscope was used to capture images of the chromosomes with z-sections spaced by 0.2μm. Images were processed by deconvolution and quick projection then mean signal intensity quantified across centromere regions as shown in Figures 5J–5L, using the 4-pixel wide line tool in ImageJ from centromere to centromere (defined by the position of the CREST foci).

The antibodies used were α-PICH,[10] rat α-DYKDDDDK (#200474-21, Agilent) for FLAG signals, 5F8 α-RFP (#RMA5F8, Bulldog Bio), α-CENP-C (#PD030, MBL), α-H3K27me3 (Upstate, 07—449), CREST serum (Cortex

Biochem, CS1058), goat α-rabbit IgG Alexa Fluor 488 (#A11034, Molecular probes/Life Technologies), goat α-rat IgG Alexa Fluor 568 (#A11077, Molecular probes/Life Technologies, Invitrogen), goat α-guinea pig IgG Alexa Fluor 647 (#A21450, Molecular probes/Life Technologies).

Morphological quantification of TopoII distribution with wndchrm

Images for wndchrm analyses were acquired from live cells expressing fluorescent TopoIIα, as described above. For quantification of morphological similarities/dissimilarities, a supervised machine learning algorithm, wndchrm (weighted neighbor distance using a compound hierarchy of algorithms representing morphology) was used, as previously described.[38–41] For the mCherry-TopoIIα wt and its mutant proteins in Figures 4D–4E, 30 images for each kind were collected, and randomly subdivided into two subgroups. For Figure S7A, 6, 8, and 10 images of mCherry-TopoIIα and mCherry-TopoIIα Y1521A were used. For Figure S7B, 30, 40, 50, 60 and 70 images and for Figure S7C, 10, 20, 30,40 and 50 cells of TopoIIα in the control and GSK-343/A-196 treated cells were used as specified. Morphological feature values of the image were automatically assigned by training a machine. For each test, cross-validation tests were automatically repeated 20 times using 70% of images as training and 30% of images as test among the provided dataset. The options used for wndchrm analysis were a large feature set of 2919 (-l) and multi-processors (-m). Morphological distances between two classes (class A and class B) were calculated as the Euclidean distances [$d=\sqrt{\sum}(A-B)2$] with the values in a class probability matrix obtained from the cross validations. pP values were also provided by two-sided Student's t-tests for each of the comparisons. Phylogenies were created with the PHYLIP package ver. 3.67,[42,43] using pairwise class similarity values computed by wndchrm.

Mono-nucleosome pull-down assays

Recombinant S-tagged TopoII-CTD proteins were loaded on S-protein Agarose beads (#69704, EMD Millipore/Novagen) by incubating them together overnight. Log phase chromatin was isolated from DLD-1 cells after cell lysis using lysis buffer (as stated in the previous section for chromosome isolation) and centrifugation after loading on with 20% glycerol cushion. The isolated chromatin was salt extracted using high salt buffer (400 mM NaCl, 18 mM β-Glycerophosphate, 20 mM HEPES (pH 7.7), 5 mM EDTA, 5 mM EDTA and 5% glycerol) and digested in Micrococcal Nuclease (MNase) buffer (50 mM NaCl, 20 mM HEPES (pH 7.7), 5% glycerol, 5 mM $CaCl_2$) with MNase (#M0247S, New England Biolabs). The obtained digest (mononucleosomes) was incubated with the beads coated with the proteins for 1h at 22°C. The beads were then washed with 1X TBS-T containing 250 mM NaCl and the results were analyzed using Western Blotting. Additionally, a fourth of the beads were treated with half-diluted salt extraction buffer containing 10% SDS and 0.5μl Proteinase-K. These samples were run on a DNA gel and the size of the input and bound digest were verified. Representative input and bound digest are shown in Figure S1B.

The primary antibodies used for analyses included α-H3K27me2 (#ab24684, abcam), α-H3K27me3 (#C36B11, Cell Signaling Technology), α-H3K27me3 (#61018, Active Motif), α-H3 (#96C10, Cell Signaling Technology), α-H4 (#61521, Active Motif) α-H4K20me3 (#39671, Active Motif). For visualizing the S-tagged bait, S-protein HRP conjugate (#69047, EMD Millipore/Novagen) was used followed by chemiluminescence substrate Pico PLUS (#34577, Thermo Scientific Protein Biology).

The Western Blot signals were visualized using the LI-COR Odyssey Fc machine and the band intensities were analyzed using the Image Studio Lite software. Each of the band intensities for histone signal were normalized with respect to the S-HRP (bait signal) for the corresponding sample. The intensity of histone/bait values was then recorded in Graphpad prism software using which statistical analyses were performed.

Methyl transferase inhibitor addition conditions and assays with inhibitor treatment

TopoIIα-AID cells engineered with hH11-Tet-ON-mCherry- TopoIIα wt were used for optimization assays. These cells were used without any Aux or Dox treatment. GSK-343(#A3449, APExBIO) or A-196 (#18317, Cayman chemical) was diluted to desired concentration from the stock in DMSO. Inhibitors was added to the culture at 1:1000 from each of the above-mentioned dilutions to obtain final concentration of the inhibitor. The inhibitor was added following wash off of the cells from Thymidine. Equal amounts of DMSO were added to control cells. Subsequently 8.5h later, the cells were fixed with 4% pFA, permeabilized with methanol for staining or isolated mitotic chromosomes for Western Blotting as described above. DNA was visualized using DAPI.

For UFB assay in Figure 6 with endogenous TopoIIα depletion and exogenously expressing mCherry TopoIIα-wt/mutants, the inhibitor was diluted to 16mM concentration from the stock then 1:4000 GSK-343 (from 16 mM) was added to obtain final concentration of 4 μM. This higher dilution factor was chosen to further reduce the amount of DMSO added to the cells along with the inhibitor (since Aux and Dox are also diluted in DMSO). Equal amounts of DMSO were added to control cells. The cells were then similarly fixed and stained as stated above with antibodies were α-PICH,[10] 5F8 α-RFP (#RMA5F8,Bulldog Bio), α-CENP-C (#PD030, MBL), goat α-rabbit IgG Alexa Fluor 488 (#A11034, Molecular probes/Life Technologies), goat α-rat IgG Alexa Fluor 568 (#A11077, Molecular probes/Life Technologies), goat α-guinea pig IgG Alexa Fluor 647 (#A21450, Molecular probes/Life Technologies).

QUANTIFICATION AND STATISTICAL ANALYSIS

The quantifiable data was analyzed for statistical significance using GraphPad Prism software (version 8). Based on the data itself, either the one-way ANOVA or paired two-tailed t-test was employed followed by suitable post-hoc tests where applicable. Information about the statistical analysis performed, is provided in the figure legends in depth.